PHYSICAL REVIEW D **76,** 125025 (2007)

Dynamics of domain wall networks

Minoru Eto,[1,2,*] Toshiaki Fujimori,[3,†] Takayuki Nagashima,[3,‡] Muneto Nitta,[4,§] Keisuke Ohashi,[5,‖] and Norisuke Sakai[3,¶]

[1]*INFN, Sezione di Pisa, Largo Pontecorvo, 3, Ed. C, 56127 Pisa, Italy*

[2]*Department of Physics, University of Pisa Largo Pontecorvo, 3, Ed. C, 56127 Pisa, Italy*

[3]*Department of Physics, Tokyo Institute of Technology, Tokyo 152-8551, Japan*

[4]*Department of Physics, Keio University, Hiyoshi, Yokohama, Kanagawa 223-8521, Japan*

[5]*Department of Applied Mathematics and Theoretical Physics, University of Cambridge, CB3 0WA, United Kingdom*

(Received 7 August 2007; published 26 December 2007)

Networks or webs of domain walls are admitted in Abelian or non-Abelian gauge theory coupled to fundamental Higgs fields with complex masses. We examine the dynamics of the domain wall loops by using the moduli approximation and find a phase rotation induces a repulsive force which can be understood as a Noether charge of Q-solitons. Non-Abelian gauge theory allows different types of loops which can be deformed to each other by changing a modulus. This admits the moduli geometry like a sandglass made by gluing the tips of the two cigar-(cone-)like metrics of a single triangle loop. We conclude that the sizes of all loops tend to grow for a late time in general models with complex Higgs masses, while the sizes are stabilized at some values once triplet masses are introduced for the Higgs fields. We also show that the stationary motion on the moduli space of the domain wall webs represents $1/4$ Bogomol'nyi-Prasad-Sommerfield Q-webs of walls.

DOI: 10.1103/PhysRevD.76.125025 PACS numbers: 11.27.+d, 11.25.−w, 11.30.Pb, 12.10.−g

I. INTRODUCTION

In various areas of physics, many kinds of topological defects are expected to be produced at a phase transition via the Kibble mechanism [1]. More than two extended objects like cosmic strings or domain walls intersect or meet with angles in general, and therefore such a production inevitably results in networks or webs of these objects [2]. In condensed matter physics several examples have been observed, while it is not the case of particle physics, astrophysics, or cosmology. Previously cosmic string junctions were suggested to be a seed of galaxy formation. Although such a possibility has been denied by recent cosmic microwave background data, it is argued that they may still play a certain role. A domain wall network was proposed to explain dark matter/energy [3]. Future observation of such defect networks in our Universe certainly deserves to be explored. Usually dynamics of these networks have been studied by computer simulation. On the other hand, in the case of particlelike solitons such as monopoles, the analytic method of the moduli space (geodesic) approximation has been developed [4,5]. By this their low-energy dynamics can be described as geodesics of the moduli space of these solitons. Therefore the determination of the moduli space is crucial for this task. In a previous paper [6] we have successfully constructed the moduli space of domain wall networks in a certain model which allows a supersymmetric generalization. Supersymmetry is expected to exist in the early Universe so this situation is realistic.

In this paper we will work out the dynamics of domain wall networks using the moduli space approximation. We find that the sizes of all loops tend to grow for late time in general models with complex Higgs masses, while the sizes are stabilized at some values once triplet masses are introduced for the Higgs fields. To the best of our knowledge this is the first example to discuss the dynamics of a composite system of solitons analytically.[1] Our model here is a $U(N_C)$ gauge theory coupled to N_F Higgs fields in the fundamental representation, which can be extended to possess $\mathcal{N} = 2$ supersymmetry in $3 + 1$ dimensions. This model has been recently studied extensively because it allows many kinds of Bogomol'nyi-Prasad-Sommerfield (BPS) solitons; see [8–10] for a review. Vacua are isolated and disconnected in theories with the number of flavors more than the number of color, $N_F > N_C$, and with nondegenerate masses for the Higgs fields [11]. Parallel multiple domain wall solutions exist as $1/2$ BPS states when the Higgs masses are real and nondegenerate. By introducing the method of the moduli matrix [9,12], *analytic* solutions of these domain walls were constructed in the strong gauge coupling limit [7] (see [13] for domain walls in $U(1)$ gauge theory). This method was then applied to construct vortex solutions [14], vortex-strings stretched between parallel domain walls [15], and instantons inside a

*minoru@df.unipi.it
†fujimori@th.phys.titech.ac.jp
‡nagashi@th.phys.titech.ac.jp
§nitta@phys-h.keio.ac.jp
‖K.Ohashi@damtp.cam.ac.uk
¶nsakai@th.phys.titech.ac.jp

[1]We have analyzed analytically compressed walls which appear as limiting configurations of multiple parallel walls compressed to each other [7]. Although these configurations may be regarded as composite solitons, they can be obtained as a smooth limiting point within a moduli space of multiple parallel walls, and do not present qualitatively new features unlike our present case of the $1/4$ BPS webs of walls.

vortex-sheet [16]. Finally the most general *analytic* solutions of 1/4 BPS networks (webs) of domain walls have been constructed in models with complex nondegenerate Higgs masses [17–19].[2] These solutions contain full moduli of a network with arbitrary numbers of loops and external legs of walls. The effective Kähler potential of 1/2 BPS solitons was constructed in the superfield formalism [22], and then it has been generalized to the case of domain wall networks [6]. The zero modes of external legs are non-normalizable and have to be fixed to discuss dynamics, while zero modes corresponding to loop size and associated internal phase are normalizable and appear as massless fields in the effective theory. We have constructed the effective Kähler potential and the metric of the simplest triangle loop in $U(1)$ gauge theory coupled with $N_F = 4$ Higgs scalars and have found that the metric has a geometry between a cone and a cigar [6]. This metric is rather nontrivial since it is regular on the tip although it corresponds to a shrinking loop. Therefore it is expected to describe a smooth bounce of the loop.

In this paper we discuss the dynamics of loops of domain walls in 3 + 1 dimensions for (1) a triangle single loop in the simplest model of $N_C = 1$ and $N_F = 4$, (2) a double loop in the model with $N_C = 1$ and $N_F = 6$, and (3) a non-Abelian loop in the model with $N_C = 2$ and $N_F = 4$. This paper is organized as follows. In Sec. II we summarize the previous results on the construction of domain wall networks and the effective action on them. The effective action describes the moduli dynamics of the domain wall networks. Notice that domain wall networks are codimension two defects so that in 3 + 1 dimensional space-time they trivially extend along one spatial direction x^3 perpendicular to the x^1, x^2 plane where the domain walls form the networks. If one wants to avoid an infinite volume of domain walls owing to the infinite extension along the x^3 axis, one may simply dimensionally reduce the model to 2 + 1 dimensions. However, moduli dynamics of the domain wall network still makes sense even in 3 + 1 dimensions in the following way. Let us suppose that the deformations along the x^3 axis are small enough in comparison with those along the x^1, x^2 axes. In such a situation our analysis in this paper is also valid in 3 + 1 dimensions.

In Sec. III we first investigate the dynamics of the single triangle loop. The moduli metric allows the $U(1)$ isometry whose orbit is parametrized by a Nambu-Goldstone mode of the flavor symmetry spontaneously broken by the configuration. Associated with this isometry, a conserved charge Q exists in the general motion of the moduli space. When $Q = 0$, a motion of a shrinking loop is bounced and the phase is rotated with the angle π after the loop completely shrinks. When $Q \neq 0$ a shrinking loop is bounced at the minimum size of the loop determined by Q.

In Sec. IV we investigate the dynamics of double loop. In this case there exist two conserved charges Q_1 and Q_2 corresponding to the phases of the two loops. Both loops will grow after their sizes bounce at the minimum irrespective of their Q-charges.

In Sec. V we work out the dynamics of a non-Abelian loop. In this case there exist two different configurations of nonplanar webs with a non-Abelian loop, which can be deformed to each other by changing a modulus. The moduli space geometry looks like a sandglass which is made by gluing the tips of the two metrics of a single triangle loop. Each region of the sandglass metric corresponds to the configuration of each non-Abelian loop. Depending on the value of the conserved charge Q one configuration can or cannot change to the other configuration.

In Sec. VI we turn on the triplet masses for the Higgs fields. In the context of field theory with eight supersymmetry charges this is possible in three space-time dimensions. We find the third masses induce the attractive force for the loop size whereas the Q-charge induces the repulsive force. Then the size of the loop is stabilized at some value where two kinds of forces are balanced. This mechanism to stabilize the size is the same as the one of the Q-lumps in nonlinear sigma models with a potential term [23–25]; the size of Q-lumps are stabilized by the Q-charge and the masses. Also, it was shown in [26] that a 1/4 BPS dyon can be understood as stationary motion in the moduli space of BPS monopoles with a potential term induced by the masses. The dyonic instanton is also understood as stationary motion in the moduli space of instantons [27]. In the same way, our motion in the moduli space of the domain wall webs suggests BPS dyonic extension of domain wall webs. In fact it has been previously shown in [25] that the configuration of Q-domain wall webs is again 1/4 BPS (but not 1/8 BPS) and is stable. We reexamine this interpretation in this section.

Section VII is devoted to the conclusion and discussion. The implication of our work to cosmology is briefly discussed.

II. EFFECTIVE ACTION OF DOMAIN WALL NETWORKS

A. BPS equations for domain wall networks

Let us here briefly present our model (see [9] for a review), which admits 1/4 BPS webs of domain walls. We consider the bosonic part of 3 + 1 dimensional $\mathcal{N} = 2$ supersymmetric $U(N_C)$ gauge theory with N_F ($> N_C$) massive hypermultiplets in the fundamental representation. Here the bosonic components in the vector multiplet are gauge fields W_M ($M = 0, 1, 2, 3$), the real scalar fields Σ_α ($\alpha = 1, 2$) in the adjoint representation, and those in the hypermultiplet are the $SU(2)_R$ doublets of the complex

[2] In $\mathcal{N} = 1$ supersymmetric field theories, junctions of domain walls were previously found to be 1/4 BPS states preserving only a quarter of supersymmetry [20]. Exact solutions of wall junctions were constructed in [21]. See [6] for more complete references of domain wall junctions in $\mathcal{N} = 1$ supersymmetric field theories.

scalar fields H^i $(i = 1, 2)$, which we express as $N_C \times N_F$ matrices. After eliminating the auxiliary fields, we obtain the bosonic part of the Lagrangian as

$$\mathcal{L} = \mathrm{Tr}\Big[-\frac{1}{2g^2} F_{MN}F^{MN} + \frac{1}{g^2}\sum_{\alpha=1}^{2} \mathcal{D}_M\Sigma_\alpha \mathcal{D}^M\Sigma_\alpha + \mathcal{D}_M H^i (\mathcal{D}^M H^i)^\dagger \Big] - V, \tag{2.1}$$

$$V = \mathrm{Tr}\Big[\frac{1}{g^2}\sum_{a=1}^{3}(Y^a)^2 + \sum_{\alpha=1}^{2}(H^i M_\alpha - \Sigma_\alpha H^i) \times (H^i M_\alpha - \Sigma_\alpha H^i)^\dagger - \frac{1}{g^2}[\Sigma_1, \Sigma_2]^2 \Big], \tag{2.2}$$

where we have defined $Y^a \equiv \frac{g^2}{2}(c^a \mathbf{1}_{N_C} - (\sigma^a)^j{}_i H^i (H^j)^\dagger)$ with g the gauge coupling for $U(N_C)$ gauge theory, and c^a an $SU(2)_R$ triplet of the Fayet-Iliopoulos (FI) parameters. In the following, we choose the FI parameters as $c^a = (0, 0, c > 0)$ by using $SU(2)_R$ rotation without loss of generality. Here we use the space-time metric $\eta_{MN} = \mathrm{diag}(+1, -1, -1, -1)$ and M_α are real diagonal mass matrices, $M_1 = \mathrm{diag}(m_1, m_2, \cdots, m_{N_F})$, $M_2 = \mathrm{diag}(n_1, n_2, \cdots, n_{N_F})$. The covariant derivatives are defined as $\mathcal{D}_M\Sigma = \partial_M\Sigma + i[W_M, \Sigma]$, $\mathcal{D}_M H^i = (\partial_M + iW_M)H^i$, and the field strength is defined as $F_{MN} = -i[\mathcal{D}_M, \mathcal{D}_N] = \partial_M W_N - \partial_N W_M + i[W_M, W_N]$.

If we turn off all the mass parameters, the vacuum manifold is the cotangent bundle over the complex Grassmannian $T^*Gr_{N_F,N_C}$ [28]. Once the mass parameters $m_A + in_A$ $(A = 1, \cdots N_F)$ are turned on and chosen to be fully nondegenerate ($m_A + in_A \neq m_B + in_B$ for $A \neq B$), almost all points of the vacuum manifold are lifted and only ${}_{N_F}C_{N_C} = N_F!/[N_C!(N_F - N_C)!]$ discrete points on the base manifold Gr_{N_F,N_C} are left to be the supersymmetric vacua [11]. This choice of the mass parameters breaks the $SU(N_F)$ flavor symmetry to $U(1)^{N_F-1}$. Each vacuum is characterized by a set of N_C different indices $\langle A_1, \cdots, A_{N_C}\rangle$, $1 \le A_1 < \cdots < A_{N_C} \le N_F$, which we will often abbreviate as $\langle A_r\rangle$ in the following. In these vacua, the vacuum expectation values are determined as

$$\langle H^{1rA}\rangle = \sqrt{c}\,\delta^{A_r}_A, \qquad \langle H^{2rA}\rangle = 0, \qquad \langle\Sigma\rangle = \mathrm{diag}(m_{A_1} + in_{A_1}, \cdots, m_{A_{N_C}} + in_{A_{N_C}}), \tag{2.3}$$

where r is the color index running from 1 to N_C, the flavor index A runs from 1 to N_F, and Σ is the complex adjoint scalar defined by $\Sigma \equiv \Sigma_1 + i\Sigma_2$.

The 1/4 BPS equations for webs of walls interpolating the discrete vacua (2.3) can be obtained by the usual Bogomol'nyi completion of the energy density as [17,18]

$$F_{12} = i[\Sigma_1, \Sigma_2], \qquad \mathcal{D}_1\Sigma_2 = \mathcal{D}_2\Sigma_1, \qquad \mathcal{D}_1\Sigma_1 + \mathcal{D}_2\Sigma_2 = Y^3, \tag{2.4}$$

$$\mathcal{D}_1 H^1 = H^1 M_1 - \Sigma_1 H^1, \qquad \mathcal{D}_2 H^1 = H^1 M_2 - \Sigma_2 H^1. \tag{2.5}$$

Here we consider static configurations which are independent of x_3, so we set $\partial_0 = \partial_3 = 0$ and $W_0 = W_3 = 0$. Furthermore, we take $H^2 = 0$ because it always vanishes for the 1/4 BPS solutions. The Bogomol'nyi energy bound is given by

$$\mathcal{E} \ge \mathcal{Y} + \mathcal{Z}_1 + \mathcal{Z}_2 + \partial_\alpha J_\alpha, \tag{2.6}$$

where the central (topological) charge densities which characterize the solutions are of the form

$$\mathcal{Y} = \frac{2}{g^2}\partial_\alpha \mathrm{Tr}(\epsilon^{\alpha\beta}\Sigma_2\mathcal{D}_\beta\Sigma_1), \qquad \mathcal{Z}_1 = c\partial_1 \mathrm{Tr}\Sigma_1, \qquad \mathcal{Z}_2 = c\partial_2 \mathrm{Tr}\Sigma_2. \tag{2.7}$$

The topological charges are defined by

$$T_w \equiv \int d^2x(\mathcal{Z}_1 + \mathcal{Z}_2), \qquad Y \equiv \int d^2x\,\mathcal{Y}. \tag{2.8}$$

Here T_w corresponds to the energy of domain walls and Y corresponds to the energy of domain wall junctions. Since energy of domain walls means tension times the length of the walls, this quantity is divergent. On the other hand Y has a finite value, and we call this charge as the junction charge or the Hitchin charge. Note that the integration of the fourth term $\partial_\alpha J_\alpha = \partial_\alpha \mathrm{Tr}[H^1(M_\alpha H^{1\dagger} - H^{1\dagger}\Sigma_\alpha)]$ in Eq. (2.6) does not contribute to the topological charges.

The 1/4 BPS equations Eq. (2.4) and Eq. (2.5) [17,18] can be solved as follows. First, since the first two equations in Eq. (2.4) give an integrability condition for the two operators $\mathcal{D}_\alpha + \Sigma_\alpha$ $(\alpha = 1, 2)$, W_α and Σ_α can be written as

$$\Sigma_\alpha + iW_\alpha = S^{-1}\partial_\alpha S. \tag{2.9}$$

Here, $S(x^1, x^2) \in GL(N_C, \mathbf{C})$ is a matrix valued function. Secondly, Eq. (2.5) can be solved as

$$H^1 = S^{-1}H_0 e^{M_1x^1 + M_2x^2}. \tag{2.10}$$

Here H_0, which we call "moduli matrix," is an $N_C \times N_F$ constant complex matrix of rank N_C, and contains all the moduli parameters of solutions. Any sets of S and moduli matrix H_0 related by the following V-transformation are physically equivalent since they do not change the physical configuration:

$$H_0 \to VH_0, \qquad S(x^1, x^2) \to VS(x^1, x^2), \qquad V \in GL(N_C, \mathbf{C}). \tag{2.11}$$

Finally, the last equation in Eq. (2.4) can be converted, by using an $N_C \times N_C$ matrix valued function defined by

$$\Omega(x^1, x^2) \equiv SS^\dagger, \tag{2.12}$$

to the following equation:

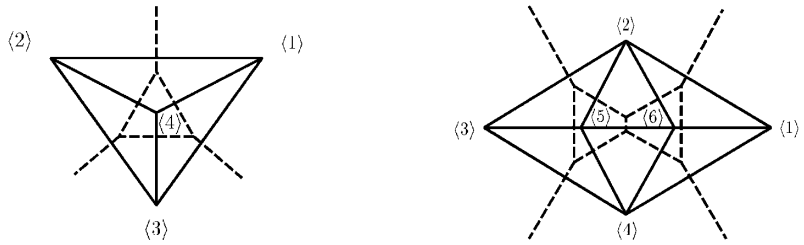

(a) triangle loop in $N_C = 1$, $N_F = 4$ model (b) double loop in $N_C = 1$, $N_F = 6$ model

FIG. 1. Grid diagram and web diagram in Abelian gauge theory.

$$\frac{1}{cg^2}(\partial_\alpha(\Omega^{-1}\partial_\alpha\Omega)) = \mathbf{1}_{N_C} - \Omega^{-1}\Omega_0, \tag{2.13}$$

where $\Omega_0 \equiv \frac{1}{c}H_0 e^{2(M_1x^1+M_2x^2)}H_0^\dagger$. This equation is called the master equation for webs of walls. Since $H^1H^{1\dagger} - c\mathbf{1}_{N_C} = 0$ in vacuum regions, the solution $\Omega(x^1, x^2)$ of the master equation should approach Ω_0 near the vacuum regions. It determines S for a given moduli matrix H_0 up to gauge transformations and then the physical fields can be obtained through Eqs. (2.9) and (2.10).

There is a useful diagram to understand the structure of webs of walls, which is called the grid diagram [17,18]. The grid diagram is a convex polygon in the complex plane $\mathrm{Tr}\langle\Sigma\rangle$ ($\Sigma \equiv \Sigma_1 + i\Sigma_2$). A vacuum point labeled by $\langle A_1 \cdots A_{N_C}\rangle$ corresponds to the vertex of the convex polygon plotted at $\mathrm{Tr}\langle\Sigma\rangle = \sum_{r=1}^{N_C}(m_{A_r} + in_{A_r})$. For each edge connecting two vertices, there is a domain wall interpolating the two vacua and each triangle corresponds to a 3-pronged domain wall junction. Some examples of grid diagrams are shown in Figs. 1 and 2. In non-Abelian gauge theory, two vacua with only one different label such as $\langle \ldots A\rangle$ and $\langle \ldots B\rangle$ can be connected while two with $\langle \ldots AB\rangle$ and $\langle \ldots CD\rangle$ are forbidden to be connected. If there are several ways to connect the vacuum points, we obtain different configurations as shown in Fig. 2. By varying the moduli parameters, we can move one configuration to another one.

One can easily read physical information about domain walls and junctions from the grid diagram. The tension of the domain wall is proportional to the length of the corresponding edge of the grid diagram. More precisely, for a domain wall interpolating between vacuum $\langle \ldots A\rangle$ and vacuum $\langle \ldots B\rangle$, the tension is given by

$$T^{\langle\ldots A\rangle\langle\ldots B\rangle} = c|\vec{m}_A - \vec{m}_B|, \tag{2.14}$$

where $\vec{m}_A$, $\vec{m}_B$ are two component vectors such that $\vec{m}_A = (m_A, n_A)$, $\vec{m}_B = (m_B, n_B)$. Furthermore the magnitude of the junction charge is proportional to the area of the corresponding triangle and its sign can be read off from the vacuum labels. If the junction interpolates three different vacua with labels such as $\langle \ldots A\rangle\langle \ldots B\rangle\langle \ldots C\rangle$, this junction is called an "Abelian junction," and its junction charge is given by

$$Y^{\langle\ldots A\rangle\langle\ldots B\rangle\langle\ldots C\rangle} = -\frac{|\Delta_{[ABC]}|}{g^2}, \tag{2.15}$$

where we have defined $\Delta_{[ABC]}$ as

$$\Delta_{[ABC]} = \vec{m}_A \times \vec{m}_B + \vec{m}_B \times \vec{m}_C + \vec{m}_C \times \vec{m}_A, \tag{2.16}$$

which is twice the area of the triangle in the grid diagram. The junction charge above is negative, and can be interpreted as the binding energy of domain walls at the junction point. On the other hand, if the junction interpolates three vacua with labels such as $\langle \ldots AB\rangle\langle \ldots BC\rangle\langle \ldots AC\rangle$, this junction is called a "non-Abelian junction," and its junction charge is given by

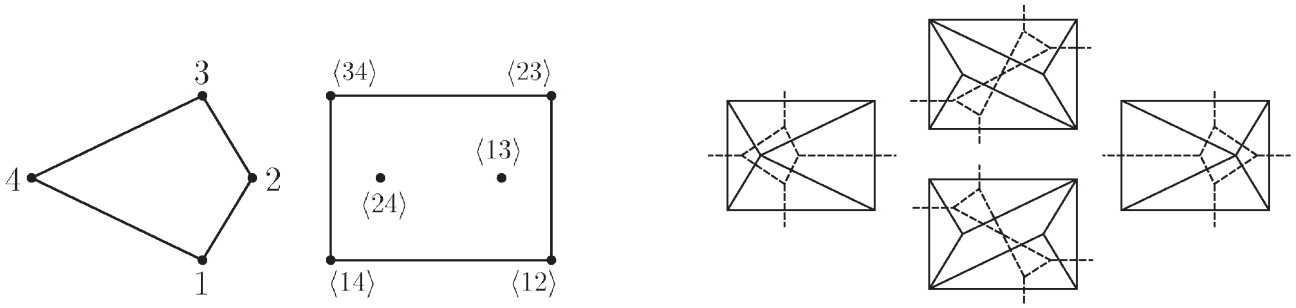

(a) mass arrangement and vacuum points (b) non-Abelian loop in $N_C = 2$, $N_F = 4$ model

FIG. 2. Grid diagram and web diagram in non-Abelian gauge theory.

$$Y^{\langle \ldots AB\rangle\langle \ldots BC\rangle\langle \ldots CA\rangle} = \frac{|\Delta_{[ABC]}|}{g^2}. \tag{2.17}$$

This is positive, and can be interpreted as the Hitchin charge of the Hitchin system. The details can be seen in [18].

In order to extract concrete information from the moduli matrix H_0, it is useful to denote $\det H_0^{\langle A_r\rangle} = \exp(a^{\langle A_r\rangle} + ib^{\langle A_r\rangle})$, where $H_0^{\langle A_r\rangle}$ is an $N_C \times N_C$ minor matrix whose elements are given by $(H_0^{\langle A_r\rangle})^{st} = (H_0)^{sA_t}$. Defining the weight $\mathcal{W}^{\langle A_r\rangle}$ of the vacuum $\langle A_r\rangle = \langle A_1 A_2 \cdots A_{N_C}\rangle$ by

$$\mathcal{W}^{\langle A_r\rangle}(x^1, x^2) \equiv \sum_{r=1}^{N_C} (m_{A_r} x^1 + n_{A_r} x^2) + a^{\langle A_r\rangle}, \tag{2.18}$$

we can write the determinant of Ω_0 as

$$\det\Omega_0 = \det\left(\frac{1}{c} H_0 e^{2(M_1 x^1 + M_2 x^2)} H_0^\dagger\right) = \frac{1}{c^{N_C}} \sum_{\langle A_r\rangle} e^{2\mathcal{W}^{\langle A_r\rangle}}. \tag{2.19}$$

If only one of the weight $\mathcal{W}^{\langle A_r\rangle}$ is nonzero, we can show that the configuration is the vacuum labeled by $\langle A_r\rangle$. Since the solution of the master equation Ω is well-approximated by Ω_0 near vacuum regions, we can estimate the position of the domain wall interpolating between vacuum $\langle A_r\rangle$ and vacuum $\langle B_r\rangle$ as a line on which the weights $\mathcal{W}^{\langle A_r\rangle}$ and $\mathcal{W}^{\langle B_r\rangle}$ are comparable:

$$\mathcal{W}^{\langle A_r\rangle} - \mathcal{W}^{\langle B_r\rangle} = \sum_{r=1}^{N_C} (m_{A_r} - m_{B_r}) x^1 + \sum_{r=1}^{N_C} (n_{A_r} - n_{B_r}) x^2 + a^{\langle A_r\rangle} - a^{\langle B_r\rangle} \simeq 0. \tag{2.20}$$

Here the other weights should be sufficiently smaller than $\mathcal{W}^{\langle A_r\rangle}$ and $\mathcal{W}^{\langle B_r\rangle}$. Hence the parameter $a^{\langle A_r\rangle} - a^{\langle B_r\rangle}$ in the moduli matrix determines the position of the domain wall. Furthermore, one can see the angle of the domain wall is determined by the mass difference between the two vacua. Notice that the domain wall line Eq. (2.20) is perpendicular to the corresponding edge of the grid diagram; see Fig. 1. So the grid diagram gives us information of the shape of the domain wall web as a dual diagram. A junction point at which three domain walls get together can also be estimated by the condition of equating the weights of three related vacua as $\mathcal{W}^{\langle A_r\rangle} \simeq \mathcal{W}^{\langle B_r\rangle} \simeq \mathcal{W}^{\langle C_r\rangle}$.

B. Effective action of domain wall networks

Once we obtain the solutions of the BPS equations Eqs. (2.4) and (2.5), we can construct a low-energy effective theory on the world volume of the domain wall networks. While all the massive modes on the background BPS solutions can be ignored at low-energies, moduli parameters (zero modes) as elements of the moduli matrix H_0 can provide massless modes which will play a main role in the effective theory. Among these zero modes, we should promote only normalizable zero modes ϕ^i to fields on the world volume of the domain wall network as

$$H_0(\phi^i) \to H_0(\phi^i(x^\mu)), \tag{2.21}$$

where x^μ ($\mu = 0, 3$) denotes the world volume coordinates of the domain wall network. On the other hand, non-normalizable zero modes which change the boundary conditions at spatial infinities cannot be promoted to fields on the world volume.

In general, the master equation Eq. (2.13) is difficult to solve. However we can obtain a general form of the effective Lagrangian for the moduli fields without solving the master equation, which has been constructed in [6]. It was found that the metric on the moduli space is a Kähler metric whose Kähler potential is given by

$$K(\phi, \bar\phi) = \int d^2x \Big[c \log \det\Omega_{\rm sol}(\phi, \bar\phi) + \frac{1}{2g^2} \mathrm{Tr}(\Omega_{\rm sol}^{-1}(\phi, \bar\phi)\partial_\alpha \Omega_{\rm sol}(\phi, \bar\phi))^2 \Big], \tag{2.22}$$

where $\Omega_{\rm sol}(\phi, \bar\phi)$ is a solution of the master Eq. (2.13). In order to get this Kähler potential, one needs to solve the Gauss's law constraint for the world volume elements of the gauge field $W_\mu(x^\mu)$,

$$\mathcal{D}_\alpha F_{\alpha 0} - i[\Sigma_\alpha, \mathcal{D}_0 \Sigma_\alpha] - i\frac{g^2}{2}(H^1 \mathcal{D}_0 H^{1\dagger} - \mathcal{D}_0 H^1 H^{1\dagger}) = 0. \tag{2.23}$$

We found [6] a generic form of the solution for Gauss's law can be expressed by derivatives with respect to the moduli fields as

$$W_\mu(x^\mu) = i(\delta_\mu S_{\rm sol}^\dagger(\phi, \bar\phi) S_{\rm sol}^{\dagger -1}(\phi, \bar\phi) - S_{\rm sol}^{-1}(\phi, \bar\phi)\delta_\mu^\dagger S_{\rm sol}(\phi, \bar\phi)), \tag{2.24}$$

where $S_{\rm sol}(\phi, \bar\phi)$ is given by $\Omega_{\rm sol}(\phi, \bar\phi) = S_{\rm sol}(\phi, \bar\phi) S_{\rm sol}(\phi, \bar\phi)^\dagger$ and the variations are defined by $\delta_\mu = \partial_\mu \phi^i \frac{\partial}{\partial \phi^i}$ and $\delta_\mu^\dagger = \partial_\mu \bar\phi^i \frac{\partial}{\partial \bar\phi^i}$. From this Kähler potential (2.22), the effective Lagrangian can be obtained as

$$\mathcal{L}^{\rm eff} = \partial_i \partial_{\bar j} K(\phi, \bar\phi) \partial^\mu \phi^i \partial_\mu \bar\phi^j = K_{i\bar j}(\phi, \bar\phi) \partial^\mu \phi^i \partial_\mu \bar\phi^j. \tag{2.25}$$

The domain wall network in Fig. 1(a) ($N_C = 1, N_F = 4$) has a single normalizable complex zero mode. To describe the zero mode, we can take the following moduli matrix without loss of generality[3]:

$$H_0 = (1, 1, 1, \phi), \quad \text{with} \quad \phi = e^w = e^{r + i\theta}. \tag{2.26}$$

[3]If we choose the central position of the loop and two relative phases carried by external walls, we can always reduce the moduli matrix H_0 for the single triangle loop to the form (2.26) using the V-transformation.

The complex parameter ϕ is the normalizable modulus parameter. One can easily see by looking at the weight of this system that its real part r changes the configuration of the triangle loop as shown in Fig. 3, and the imaginary part θ corresponds to the phase of the loop. For sufficiently large r, the size of the loop is proportional to r.

The other zero modes, the first three elements in Eq. (2.26), are non-normalizable, and have to be fixed by boundary conditions when we construct the effective theory of the domain wall network. The effective Lagrangian for the size moduli has been already constructed in [6]. The Kähler potential and the metric are smooth everywhere in terms of the complex coordinate ϕ, and the moduli space has a geometry between a cone and a cigar with a tip at $\phi = 0$ ($r = -\infty$). It was found that the Kähler potential in the strong gauge coupling limit $g^2 \to \infty$ is given as a sum of hypergeometric functions; see Eq. (3.30) of [6].

In particular the Kähler potential and the metric of the single triangle loop are given asymptotically for large $|\phi| = e^r$ by

$$K = \frac{c}{4\Delta_{[123]}}\left[\frac{1}{6\alpha_1\alpha_2\alpha_3}(\log|\phi|^2)^3 \mp \frac{1}{g^2 c}\left(\frac{|\vec{m}_{12}|^2}{\alpha_3} + \frac{|\vec{m}_{23}|^2}{\alpha_1} + \frac{|\vec{m}_{31}|^2}{\alpha_2}\right)(\log|\phi|^2)^2\right], \tag{2.27}$$

$$ds^2 = \frac{c}{\Delta_{[123]}}\left[\frac{r}{\alpha_1\alpha_2\alpha_3} \mp \frac{1}{g^2 c}\left(\frac{|\vec{m}_{12}|^2}{\alpha_3} + \frac{|\vec{m}_{23}|^2}{\alpha_1} + \frac{|\vec{m}_{31}|^2}{\alpha_2}\right)\right](dr^2 + d\theta^2), \tag{2.28}$$

where $\vec{m}_{AB} = \vec{m}_B - \vec{m}_A$ and ratios $\alpha_A \equiv \frac{1}{2\Delta_{[123]}}\epsilon_{ABC}\vec{m}_B \times \vec{m}_C$ satisfying $\alpha_1 + \alpha_2 + \alpha_3 = 1$. The minus sign in Eqs. (2.27) and (2.28) is for the triangle loop in the $U(1)$ gauge theory and the plus sign in the $U(3)$ gauge theory.[4] The corrections to the asymptotic metric have been found to be exponentially suppressed. An interesting feature is that the above asymptotic metric can be understood as the kinetic energies: the first terms in the parentheses in Eqs. (2.27) and (2.28) represent the kinetic energies of domain walls and the second (with the $\mp$ sign in front) that of junctions. Since the lengths of domain walls are proportional to r, their masses and kinetic energies have linear dependence on r. On the other hand, the junction charges are localized at the junction points, and so their kinetic energies do not depend on r. This interpretation nicely explains the sign of the second term. See Eqs. (2.15) and (2.17). This result implies that the asymptotic metric for more complicated configurations can also be obtained by computing the kinetic energies of domain walls and junctions. We will often use this result in investigating the dynamics of various domain wall networks below.

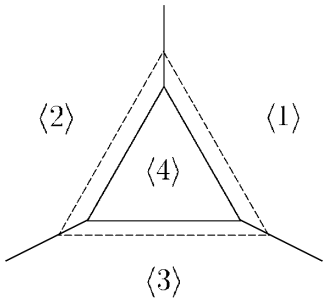

FIG. 3. The triangle loop configuration has four vacuum regions $\langle A\rangle$ ($A = 1, \cdots, 4$). We fix three complex moduli parameters which are related to positions of external walls. A unique normalizable mode is a zero mode which is related to the area of the region $\langle 4\rangle$, namely, the size of the triangle loop.

Before closing this section, let us briefly discuss another configuration closely related to the above one. When the vacua inside a loop are degenerate vacua, the loop acquires some internal moduli.[5] The asymptotic metric for the additional moduli exhibits another characteristic feature. Since the triangle loop requires at least 4 flavors that are non-degenerate, we need to take more than 4 flavors to examine a degenerate vacuum in the loop. Let us assume that mass parameters for external vacua are all nondegenerate $\vec{m}_A \neq \vec{m}_B$ for $A \neq B$ ($A, B = 1, 2, 3, 4$), and the other mass parameters corresponding to the vacuum in the loop are all degenerate $\vec{m}_A = \vec{m}_B$ for ($4 \leq A, B \leq N_F$). Such a loop configuration with the degenerate vacuum is described by the moduli matrix

$$H_0 = (1, 1, 1, \boldsymbol{\phi}), \qquad \boldsymbol{\phi} = (\phi_1, \phi_2, \cdots, \phi_{N_F-3}). \tag{2.29}$$

In this case, there exist $N_F - 3$ complex normalizable zero modes: one of them corresponds to the size and phase of the loop and the others are zero modes associated with the vacuum moduli inside the loop. We can obtain the Kähler potential K in this case, if we replace $|\phi|^2$ in Eq. (2.27) by $|\boldsymbol{\phi}|^2 \equiv |\phi_1|^2 + \cdots + |\phi_{N_F-3}|^2$. Therefore the knowledge of the Kähler potential for the $N_F = 4$ case gives a Kähler metric for this degenerate case as

$$K_{i\bar{j}} = \partial_{\phi_i}\partial_{\bar{\phi}_j}K = \delta_{ij}K'(|\boldsymbol{\phi}|^2) + \bar{\phi}_i\phi_j K''(|\boldsymbol{\phi}|^2), \tag{2.30}$$

where the prime on K denotes differentiation with respect to $|\boldsymbol{\phi}|^2$. See the appendix for a concrete example. By

[4]Here we take gauge coupling g and mass parameters for Higgs scalars (hypermultiplets) to be the same for two distinct $U(1)$ and $U(3)$ gauge theories with $N_F = 4$. They are dual in the sense that the number of vacua is equal and also their grid diagrams are congruent to each other. The duality becomes exact in the strong gauge coupling limit $g^2 \to \infty$.

[5]Domain walls with degenerate masses were studied in [29,30]. It was found that some Nambu-Goldstone modes for broken non-Abelian flavor symmetry are localized around (between) the domain walls and appear in the effective theory on them.

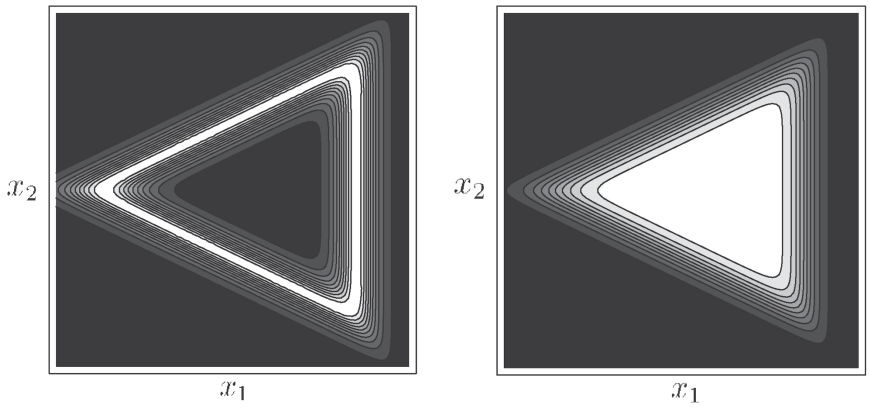

(a) size and phase moduli (b) vacuum moduli inside the loop

FIG. 4. The densities of the metric for $N_C = 1$, $N_F = 5$ in the strong coupling limit $g \to \infty$. At each point on the moduli space, the tangent space of the moduli space is orthogonally decomposed into the directions of size, phase, and two vacuum moduli inside the loop.

differentiating the leading contribution $(\log|\boldsymbol{\phi}|^2)^3$ of this Kähler potential at asymptotic region $r = \log|\boldsymbol{\phi}|^2 \gg 1$, we find that the Kähler metric contains not only terms proportional to r as in Eq. (2.28), but also terms proportional to r^2 as shown in Eq. (A5). This feature shows that among moduli fields, there are massless modes with a support extending two-dimensionally over the entire vacuum region inside the loop in the web of walls as illustrated in Fig. 4.

III. DYNAMICS OF TRIANGLE LOOP

Since we have obtained the metric on the moduli space of the triangle loop, its dynamics can be discussed as

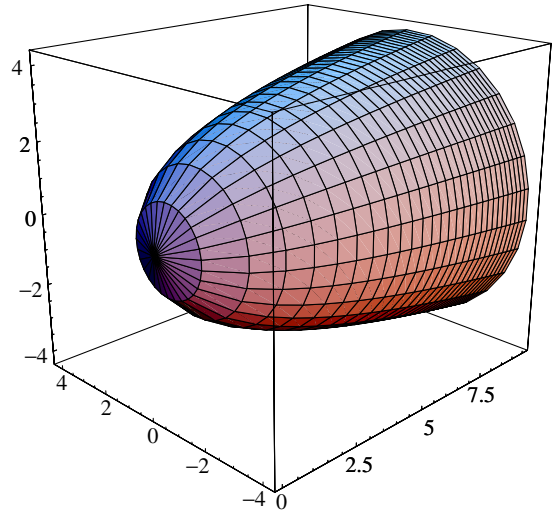

FIG. 5 (color online). The moduli space of a single triangle loop embedded in $\mathbf{R}^3$: The moduli space has a $U(1)$ isometry which corresponds to the direction of the phase modulus. The other direction can be regarded as the direction of size modulus of the loop. The tip of the moduli space corresponds to the point $\phi = 0$ where the loop shrinks completely.

geodesic motions on the moduli space. In order to avoid infinite volume of domain walls we may compactify the world volume direction or simply dimensionally reduce the model to $2 + 1$ dimensions. Such a model is obtained merely restricting the indices M, N in the Lagrangian (2.1) to 0, 1, 2. However, the analysis in the following sections is also valid in $3 + 1$ dimensions in the sense that we stressed in the introduction. The effective Lagrangian takes the form

$$L = K_{w\bar{w}}(r)\left[\left(\frac{dr}{dt}\right)^2 + \left(\frac{d\theta}{dt}\right)^2\right], \tag{3.1}$$

with $w = r + i\theta$ in Eq. (2.26). It is worth emphasizing that the moduli space is regular with positive curvature even when the loop shrinks completely. Figure 5 shows the embedding of the moduli space into 3-dimensional Euclidean space. The moduli space has a $U(1)$ isometry which originates from a linear combination of three $U(1)$ flavor symmetries. Correspondingly, there exists a conserved charge such that

$$Q \equiv \frac{\partial L}{\partial(d\theta/dt)} = 2K_{w\bar{w}}\frac{d\theta}{dt}. \tag{3.2}$$

In terms of this conserved Q-charge, the effective Lagrangian can be rewritten[6] as

$$\tilde{L} = K_{w\bar{w}}(r)\left(\frac{dr}{dt}\right)^2 - \frac{Q^2}{4K_{w\bar{w}}(r)}. \tag{3.3}$$

Here the second term can be interpreted as a potential associated with the conserved charge Q. Note that the smoothness of the Kähler metric in terms of $\phi = e^w$ means the metric $K_{w\bar{w}}$ is exponentially suppressed as $K_{w\bar{w}} \propto e^{2r} \to 0$ for $r = \mathrm{Re}w \to -\infty$. We also know the asymp-

[6]We have performed a Legendre transformation of L with respect to θ.

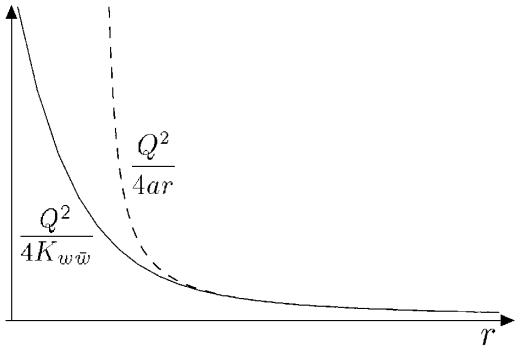

FIG. 6. Plot of the potential $V = Q^2/4K_{w\bar{w}}$ in the $g^2 \to \infty$ limit (solid line) and the asymptotic ($r \gg 1$) potential $V = Q^2/4ar$, $a = \frac{c}{2\Delta_{[123]}}\frac{1}{\alpha_1\alpha_2\alpha_3}$ (dashed line) given in Eq. (2.28). The phase rotation produces the repulsive force among the triangle loop.

totic behavior $K_{w\bar{w}} \propto r \to \infty$ for $r \to \infty$. The typical form of the potential is shown in Fig. 6. We can find that the phase rotation produces the repulsive potential among the triangle loop. This repulsive potential makes the loop expand forever, namely, the trajectory of the loop exhibits a runaway behavior. Although we are now considering the effective theory of domain wall networks, it is possible to consider domain wall networks with Q-charges in the original theory. The above runaway potential tells us that such configuration is unstable and no longer BPS. However, we will see in Sec. VI that a stable stationary point appears if we introduce another type of mass term (triplet mass). The corresponding configuration will turn out to be BPS, conserving a quarter of supercharges.

Now let us return to geodesic motions on the moduli space. We introduce an integral of motion E as an integration constant as

$$E = K_{w\bar{w}}(r)\left(\frac{dr}{dt}\right)^2 + \frac{Q^2}{4K_{w\bar{w}}(r)}, \tag{3.4}$$

corresponding to the energy associated with the motion of the zero-modes $r(t)$ and $\theta(t)$. By exploiting this conservation law of energy, we can obtain the solution of the equation of motion. The orbit of the geodesic for a given energy E is given by

$$\theta - \theta_0 = \pm \int dr \frac{Q}{\sqrt{4K_{w\bar{w}}(r)E - Q^2}}, \tag{3.5}$$

and the time dependence of the size modulus r is given by

$$t - t_0 = \pm \int dr \frac{2K_{w\bar{w}}(r)}{\sqrt{4K_{w\bar{w}}(r)E - Q^2}}. \tag{3.6}$$

If we consider the motion in the direction of smaller values of r with $Q = 0$, the geodesic is a straight line in the complex ϕ-plane and goes through the tip of the manifold $\phi = 0$ ($r = -\infty$). This motion corresponds to the bounce of the loop, that is, after the loop shrinks completely, it tends to be larger with 180° phase rotation. In the case of $Q \neq 0$, the repulsive force among the loop become stronger as the size become smaller, so that it prevents the loop from shrinking completely. Hence, there exists a minimum value of the size modulus r determined by

$$E = \frac{Q^2}{4K_{w\bar{w}}(r_{\min})}. \tag{3.7}$$

This implies that if the initial velocity of the size modulus $\frac{dr}{dt}$ is negative, the loop shrinks to its minimum size $r = r_{\min}$ and then the velocity $\frac{dr}{dt}$ changes its sign.

The large size behavior can be investigated using the asymptotic metric Eq. (2.28). First note that the second term in Eq. (2.28) can be absorbed by shifting the parameter as $r \to r \mp \alpha_1\alpha_2\alpha_3(|\vec{m}_{12}|^2/\alpha_3 + |\vec{m}_{23}|^2/\alpha_1 + |\vec{m}_{31}|^2/\alpha_2)/g^2c$. After the shift, the equation of motion for r can be solved as

$$\theta - \theta_0 = \pm \frac{Q}{2aE}\sqrt{4aEr - Q^2}, \tag{3.8}$$

$$t - t_0 = \pm \frac{1}{6aE^2}(2aEr + Q^2)\sqrt{4aEr - Q^2}, \tag{3.9}$$

where $a = \frac{c}{2\Delta_{[123]}}\frac{1}{\alpha_1\alpha_2\alpha_3}$. In the case of $Q = 0$, the above equation says $r \sim t^{2/3}$. This reflects the fact that the mass of the triangle loop is proportional to r and its velocity becomes smaller as the size of the loop becomes large. For the loop with $Q \neq 0$, the minimum size is given by $r_{\min} = Q^2/4aE$. The typical time dependence of the size modulus is shown in Fig. 7. Since our argument above is based on the asymptotic metric Eq. (2.28) which is valid for $r \gg 1$, the solution Eqs. (3.8) and (3.9) can be well trusted only when $r_{\min} = Q^2/4aE \gg 1$. Of course, the energy E should be small enough so as not to excite the massive modes.

The asymptotic potential $V = Q^2/4ar$ can be interpreted as the shift of the energies associated with the walls composing the loop. This expectation can be confirmed by the following argument. For a domain wall with tension T, the rotation of its phase induces flavor charge density ρ_Q on the world volume given by

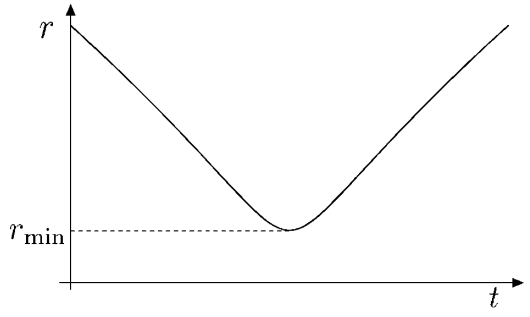

FIG. 7. The solution of the equation of motion for size modulus with $Q \neq 0$. The phase rotation produces the repulsive potential and the loop bounces back at $r_{\min} = Q^2/4aE$.

$$\rho_Q = \frac{c^2 \frac{d\theta}{dt}}{\sqrt{T^2 - c^2(\frac{d\theta}{dt})^2}} \sim \frac{c^2}{T}\frac{d\theta}{dt}. \tag{3.10}$$

In addition, the phase rotation causes a shift of the tension as

$$\Delta T = T\sqrt{1 + \rho_Q^2/c^2} - T \sim \frac{T}{2c^2}\rho_Q^2. \tag{3.11}$$

For the loop, each wall composing the loop becomes a domain wall with flavor charges by rotating the phase modulus θ. Since the tensions and lengths of the walls composing the loop are given by

$$T^{(A,4)} = c|\vec{m}_A|, \qquad l^{(A,4)} = \frac{|\vec{m}_A|}{\Delta_{[123]}}\frac{\alpha_A}{\alpha_1\alpha_2\alpha_3}r, \qquad A = 1, 2, 3, \tag{3.12}$$

the total flavor charge for the wall interpolating between $\langle A\rangle$-th and $\langle 4\rangle$-th vacua is

$$Q_A = \frac{c^2}{T^{(A,4)}}\frac{d\theta}{dt}l^{(A,4)} = \frac{c}{\Delta_{[123]}}\frac{\alpha_A}{\alpha_1\alpha_2\alpha_3}r\frac{d\theta}{dt}. \tag{3.13}$$

From this expression, we find that the total charge $Q = \sum Q_A$ agrees with Eq. (3.2) in large r limit and Q_A are given by $Q_A = \alpha_A Q$. Therefore the total shift of energy is given by

$$\sum_{A=1}^{3}\Delta T^{(A,4)}l^{(A,4)} = \sum_{A=1}^{3}\frac{T^{(A,4)}}{2c^2}\left(\frac{\alpha_A Q}{l^{(A,4)}}\right)^2 l^{(A,4)} = \frac{Q^2}{4ar}. \tag{3.14}$$

From the argument above, we can intuitively understand the reason why the phase rotation gives rise to a repulsive potential as follows: Since the shifts of tensions of the walls are proportional to ρ_Q^2 and the lengths of the walls are proportional to r, the shift of the total energy is proportional to $\rho_Q^2 r$. This fact implies that if the charge density is constant, the total energy increases as the size of the loop becomes larger. However since the conserved quantity is not the density ρ_Q but the total flavor charge Q, the density decreases in proportion to $1/r$ and hence the total energy decreases in proportion to $1/r$ as the size of the loop become larger. This is the reason why the phase rotation produces the decreasing repulsive potential.

Next, let us consider the dynamics of a triangle loop with degenerate masses. The Kähler potential can be obtained by replacing $|\phi|^2$ with $|\boldsymbol{\phi}|^2 \equiv |\phi_1|^2 + \cdots |\phi_{N_F-3}|^2$ in $K(|\phi|^2)$ and the Kähler metric of the moduli space is given in Eq. (2.30). All but the size moduli $r \equiv \log|\boldsymbol{\phi}|$ can be eliminated from the expression of energy by using the conserved charges associated with $U(N_F - 3)$ flavor symmetry. For example, the energy in the case of $N_F = 5$ takes the form (see appendix)

$$E = \frac{1}{4}\partial_r^2 K\dot{r}^2 + \frac{Q^2}{\partial_r^2 K} + \frac{|q|^2 - Q^2}{2\partial_r K}, \tag{3.15}$$

where $|q|^2 \equiv \sum_{a=1}^{3} q_a q_a$ and the conserved charges Q, q_a $(a = 1, 2, 3)$ are defined by

$$\begin{aligned} Q &= iK_{i\bar{j}}\left(\frac{d\bar{\phi}^j}{dt}\phi^i - \frac{d\phi^i}{dt}\bar{\phi}^j\right), \\ q_a &= iK_{i\bar{j}}\left(\frac{d\bar{\phi}^j}{dt}(\sigma_a)^i{}_k\phi^k - \frac{d\phi^i}{dt}\bar{\phi}^k(\sigma_a)_k{}^j\right). \end{aligned} \tag{3.16}$$

Note that these conserved charges are related as $Q = (\bar{\phi}\sigma_a\phi)q_a/|\boldsymbol{\phi}|^2$ and satisfy an inequality $Q^2 \le |q|^2$. The second and third terms in Eq. (3.15) can be interpreted as the effective potential $V(r)$ associated with the conserved charges. For large r, this potential takes the form

$$V(r) = \frac{Q^2}{4ar} + \frac{|q|^2 - Q^2}{4ar^2}. \tag{3.17}$$

The first term of the potential takes the same form as in the case of nondegenerate masses. Conversely, the second term is induced by the Noether charges associated with the vacuum moduli inside the loop. To understand intuitively the origin of the second term, we can use the same argument for the first term. What we should notice is only the fact that a part of the Noether charge q_a which has no contribution to Q is supported by the two-dimensional vacuum inside the loop, while the charge Q has one-dimensional support on the walls. Therefore we can easily rederive the behavior of the second term repulsive potential proportional to $1/r^2$. This potential can be also understood by exchange of the massless particles propagating the degenerate vacuum.

IV. DYNAMICS OF DOUBLE LOOP

We will consider the dynamics of double loop shown in Fig. 1(b) in this section. Unlike the previous example, this configuration has two normalizable zero modes which are related to the sizes of the loops and their phases. By varying the sizes of the loops, we obtain various configurations of the loops. We will first explain the configurations of the domain wall web and then discuss the dynamics of the double loop.

The model is $U(1)$ gauge theory with six hypermultiplets, and we choose six complex masses as follows (assuming a real positive value for $m > 0$):

$$M = \mathrm{diag}\left(\frac{3m}{2}, i\frac{\sqrt{3}m}{2}, -\frac{3m}{2}, -i\frac{\sqrt{3}m}{2}, \frac{m}{2}, -\frac{m}{2}\right). \tag{4.1}$$

The solution of the BPS equations Eqs. (2.4) and (2.5) is characterized by H_0, which is now six component row vector

$$H_0 = \sqrt{c}(e^{a_1+ib_1}, e^{a_2+ib_2}, e^{a_3+ib_3}, e^{a_4+ib_4}, e^{a_5+ib_5}, e^{a_6+ib_6}). \tag{4.2}$$

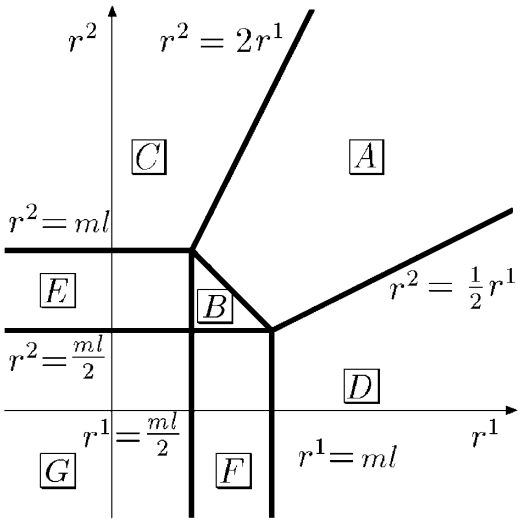

FIG. 8. Seven regions of moduli space corresponding to different patterns of configurations.

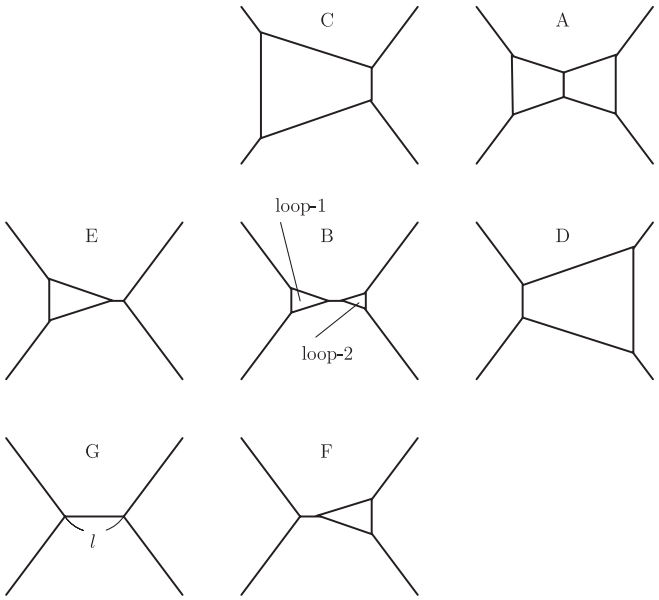

FIG. 9. Configurations of double loop.

Since the parameters a_i and b_i ($i = 1, \cdots, 4$) are related to positions and phases of external walls, these will be non-normalizable modes if these are promoted to fields, and normalizable zero modes correspond to the parameters in the fifth and sixth components of H_0. They are related to sizes of the double loop and their phases. When we consider the effective theory of the domain wall network, we have to fix four complex moduli parameters and promote two normalizable modes to fields:

$$H_0 = \sqrt{c}(1, e^{3ml/4}, 1, e^{3ml/4}, \phi^1(x^\mu), \phi^2(x^\mu)), \qquad (4.3)$$

with $\phi^i = e^{w^i} = e^{r^i + i\theta^i}$ ($i = 1, 2$). For simplicity, we have chosen a somewhat symmetric set of four complex parameters for external walls. By varying the sizes of loops, we obtain seven different patterns of web configurations as shown in Figs. 8 and 9. Let us recall the vacuum assignment depicted in Fig. 1(b) which gives the grid diagram together with the web diagram A in Fig. 9. The fixed parameter l corresponds to the length between the $\langle 1\rangle\langle 2\rangle \times \langle 4\rangle$ junction and the $\langle 2\rangle\langle 3\rangle\langle 4\rangle$ junction, in other words, the length of the $\langle 2\rangle\langle 4\rangle$ wall (internal line) of configuration G in Fig. 9. We call the left loop surrounding vacuum $\langle 5\rangle$ loop-1 and the right surrounding $\langle 6\rangle$ loop-2. In region A(B), both loop-1 and loop-2 appear as quadrangle loops (triangle loops). When the loop-1(2) grows and covers the junction $\langle 1\rangle\langle 2\rangle\langle 4\rangle$ ($\langle 2\rangle\langle 3\rangle\langle 4\rangle$), the other loop-2(1) is eaten by the loop-1(2) as C(D) in Fig. 9. In region E(F) the loop-2(1) vanishes and the triangle loop-1(2) exists. In region G both the loop-1 and loop-2 disappear.

Since the Kähler potential K is independent of θ^i, the Kähler metric $K_{i\bar{j}}$ can be written as $K_{i\bar{j}} \equiv \frac{\partial}{\partial w^i}\frac{\partial}{\partial \bar{w}^j}K = \frac{1}{4} \times \frac{\partial}{\partial r^i}\frac{\partial}{\partial r^j}K$. Then the effective Lagrangian takes the form

$$\begin{aligned} L &= K_{i\bar{j}}(r^1, r^2)\frac{dw^i}{dt}\frac{d\bar{w}^j}{dt} \\ &= K_{i\bar{j}}(r^1, r^2)\left(\frac{dr^i}{dt}\frac{dr^j}{dt} + \frac{d\theta^i}{dt}\frac{d\theta^j}{dt}\right), \end{aligned} \qquad (4.4)$$

where we have used $K_{i\bar{j}} = K_{j\bar{i}}$. In this case, there exist two conserved charges defined by $Q_i \equiv 2K_{i\bar{j}}\frac{d\theta^j}{dt}$. By using these conserved charges, the Lagrangian can be rewritten as

$$\tilde{L} = K_{i\bar{j}}(r^1, r^2)\frac{dr^i}{dt}\frac{dr^j}{dt} - \frac{1}{4}K^{\bar{j}i}(r^1, r^2)Q_iQ_j, \qquad (4.5)$$

where $K^{\bar{j}i}$ is the inverse of the metric $K_{i\bar{j}}$.

In the previous section, we have found the characteristic property of the loop, that is, the loop is apt to become larger irrespective of $Q = 0$ or $Q \neq 0$. Therefore, we expect that the loops would become larger and sit in region A in Fig. 8 after a sufficiently long time interval. Some examples of numerical solutions without flavor charges ($Q_1 = Q_2 = 0$) are shown in Fig. 10. For the initial velocities such that $\frac{dr^2}{dt} \lesssim 2\frac{dr^1}{dt}$ and $\frac{dr^2}{dt} \gtrsim \frac{1}{2}\frac{dr^1}{dt}$ (Fig. 10(a)), the orbits of the solutions are almost straight lines in r^1-r^2 plane and sit entirely in region A. For the initial velocities such that $\frac{dr^2}{dt} \gtrsim 2\frac{dr^1}{dt}$ and $\frac{dr^2}{dt} \gtrsim -\frac{dr^1}{dt}$ (Fig. 10(b)), the orbits of the solutions first enter region C, namely, one of the loops shrinks. Then, they bounce back at $r^1 = -\infty$ and return to region A. For the initial velocities such that $\frac{dr^2}{dt} \lesssim -\frac{dr^1}{dt}$ and $\frac{dr^2}{dt} \gtrsim \frac{1}{2}\frac{dr^1}{dt}$ (Fig. 10(c)), one of the loops shrinks and bounces back at $r^1 = -\infty$. Then, they enter region D and bounce at $r^2 = -\infty$, namely, the other loop shrinks to zero size. Finally, the orbits return to region A and the sizes continue to become larger.

Next, let us consider the case of the double loop with the flavor charges. Figure 11 shows an example of the potential

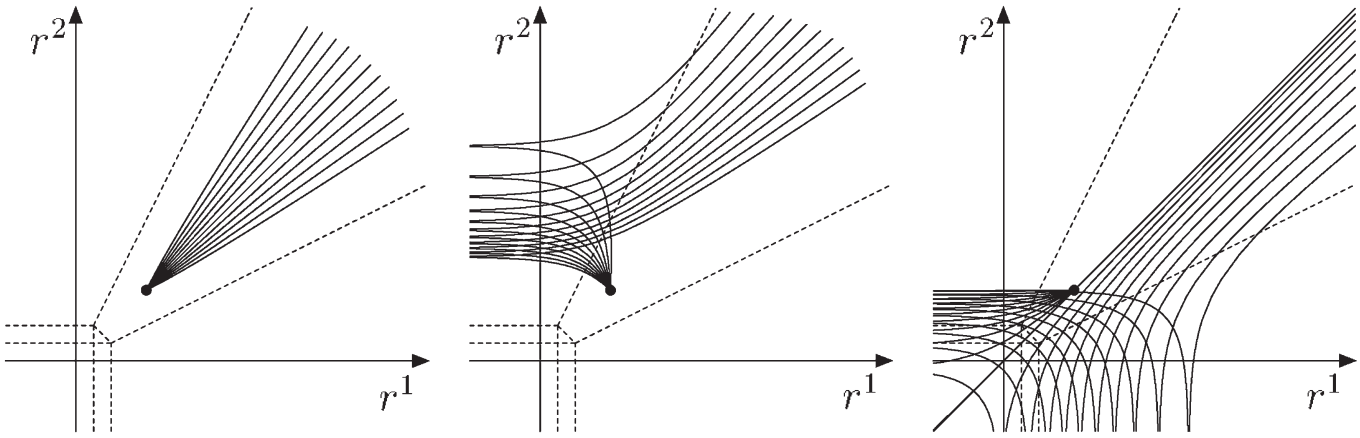

FIG. 10. Numerical solutions of the equation of motion for double loop without flavor charges. The initial state has been taken to be configuration A with the same loop size, and some orbits for various initial velocities are shown in these figures.

$V = \frac{1}{4}K^{\bar{j}i}Q_iQ_j$ and numerical solutions for the double loop with flavor charges. The potential increases rapidly outside region A and produces the repulsive force among the walls, so that any orbits of the solutions enter region A after a sufficiently long time interval and continue to become larger. Other numerical simulations also demonstrate that region A is preferable.

It is possible to know the asymptotic metric in region A for $r^1 \approx r^2 \gg ml$ by computing the kinetic energy of domain walls. The kinetic energy of domain walls implies that the asymptotic metric $r^1 \approx r^2 \gg ml$ is given by

$$ds^2 = \frac{c}{\sqrt{3}m^2}[(8r^1 - r^2)|dw^1|^2 + (8r^2 - r^1)|dw^2|^2 - (r^1 + r^2)(dw^1 d\bar{w}^2 + dw^2 d\bar{w}^1)] = \frac{5\sqrt{3}c}{2m^2}[\mathrm{Re}\mu_+|d\mu_+|^2 + \mathrm{Re}\mu_-|d\mu_-|^2], \quad (4.6)$$

where $\mu_\pm$ is defined by $\mu_\pm \equiv (1 \pm \lambda)w^1/2 + (1 \mp \lambda)w^2/2$, $\lambda \equiv 3/\sqrt{5}$. This form of the metric implies that the geodesic equation decomposes into two independent equations which can be solved as in the case of the triangle loop.

Figure 11 appears to illustrate that the trajectory of the double loop configurations can bounce back at most only twice. However, this behavior is due to the particular mass assignment of the model; namely, the center wall in configuration A is rather heavy. Let us consider a smaller mass difference between two flavors corresponding to the vacua inside the loop, such as

$$M = \mathrm{diag}\left(\frac{3m}{2}, i\frac{\sqrt{3}m}{2}, -\frac{3m}{2}, -i\frac{\sqrt{3}m}{2}, \frac{m'}{2}, -\frac{m'}{2}\right), \quad m' \ll m. \quad (4.7)$$

Then the mass of the center wall is much smaller than those

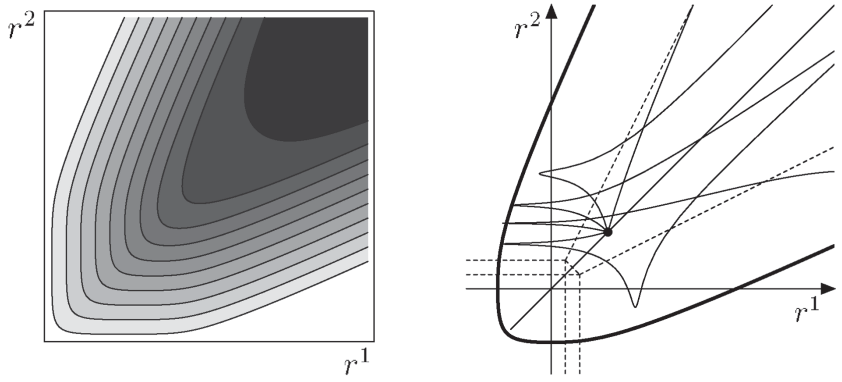

(a) Contour plot of the potential, (b) numerical solutions with flavor charges.

FIG. 11. (a) Contour plot of the potential $\log V = \log(\frac{1}{4}K^{\bar{j}i}Q_iQ_j)$. (b) Orbits of numerical solutions with flavor charges. There exists a forbidden region where the potential energy exceeds the given total energy $V(r) > E$.

of the other walls. Such mass assignment makes it possible that the double loop configuration bounces a lot of times. Moreover, if we consider the case of degenerate masses $m' = 0$, we can have configurations exhibiting as many "bounces" as one wishes. In this degenerate mass limit, the center wall is no longer visible, rather, it spreads over the entire middle vacuum region in the loop. Correspondingly, the mode also spreads over the vacuum region as in the case of a triangle loop with degenerate masses (see Fig. 4) and it describes the degrees of freedom of the degenerate vacua inside the quadrangle loop. Furthermore, it is interesting to note that the infinitely many bounces in the degenerate mass limit naturally reduces to the repulsive force, which is described by a potential similar to the second term in Eq. (3.17) with a different coefficient a. To describe the dynamics in the degenerate mass limit, we can use the expression for the energy Eq. (3.15), if the Kähler potential K is replaced by that for a quadrangle loop.

V. DYNAMICS OF NON-ABELIAN LOOP

We will next consider the dynamics of non-Abelian loop shown in Fig. 2 in this section. This configuration has four external walls, and also four internal walls which divide six vacua and constitute a quadrangle loop. After fixing the positions of external walls, one complex moduli parameter is left. The difference from the Abelian loop is that the moduli parameter controls the areas of two vacuum regions. First we will explain the configuration and moduli parameters, and then we will discuss the dynamics of the non-Abelian loop. For the details of the non-Abelian webs of walls, see [18].

The model is $U(2)$ gauge theory with $N_F = 4$ hypermultiplets, and we choose four complex mass parameters as follows:

$$M_1 + iM_2 = \mathrm{diag}\left(\frac{m}{2} - im, \frac{3m}{2}, \frac{m}{2} + im, -\frac{3m}{2}\right). \quad (5.1)$$

The complex masses and vacuum points in the $\mathrm{Tr}\langle\Sigma\rangle$ plane are shown in Fig. 2(a). The solutions of the BPS equations are characterized by a 2×4 moduli matrix H_0. It is convenient to extract the 2×2 matrix $H_0^{\langle A_1 A_2\rangle}$ defined by $(H_0^{\langle A_1 A_2\rangle})^{st} = (H_0)^{sA_t}$, $s, t = 1, 2$. Let us denote $\det H_0^{\langle A_1 A_2\rangle}$ as

$$\tau^{\langle A_1 A_2\rangle} \equiv \exp(a^{\langle A_1 A_2\rangle} + ib^{\langle A_1 A_2\rangle}) = \det H_0^{\langle A_1 A_2\rangle}. \quad (5.2)$$

These parameters are not independent but satisfy the so-called Plücker relation given by

$$\tau^{\langle 12\rangle}\tau^{\langle 34\rangle} - \tau^{\langle 13\rangle}\tau^{\langle 24\rangle} + \tau^{\langle 14\rangle}\tau^{\langle 23\rangle} = 0. \quad (5.3)$$

Each parameter $a^{\langle A_1 A_2\rangle}$ corresponds to the area of the vacuum region $\langle A_1 A_2\rangle$ and $b^{\langle A_1 A_2\rangle}$ to the associated phase as before. In order to fix four external walls, we set four complex moduli parameters as

$$a^{\langle 12\rangle} = a^{\langle 34\rangle} = -a^{\langle 14\rangle} = -a^{\langle 23\rangle} = \frac{mL}{4}, \quad (5.4)$$

$$b^{\langle 12\rangle} = b^{\langle 34\rangle} = b^{\langle 14\rangle} = b^{\langle 23\rangle} = 0. \quad (5.5)$$

The parameter L controls the positions of the external walls and the shape of the quadrangle loop as shown in Fig. 12. The remaining moduli parameters are $\tau^{\langle 13\rangle}$ and $\tau^{\langle 24\rangle}$, which determine the size of the loop. We introduce two complex parameters $u, v \in \mathbf{C}$ as

$$a^{\langle 13\rangle} + ib^{\langle 13\rangle} = (u + v)\frac{mL}{4}, \quad (5.6)$$

$$a^{\langle 24\rangle} + ib^{\langle 24\rangle} = (u - v)\frac{mL}{4}. \quad (5.7)$$

The parameter u is fixed by the Plücker relation Eq. (5.3). In the following, we take L sufficiently large, $L \gg 1/m$, so that the equation Eq. (5.3) determines the parameter u as $u \simeq 1$. Then the only parameter left is v, which we denote as $v \equiv s + i\theta$. The moduli parameter s controls the areas of two vacua $\langle 13\rangle$ and $\langle 24\rangle$, and three patterns of webs with

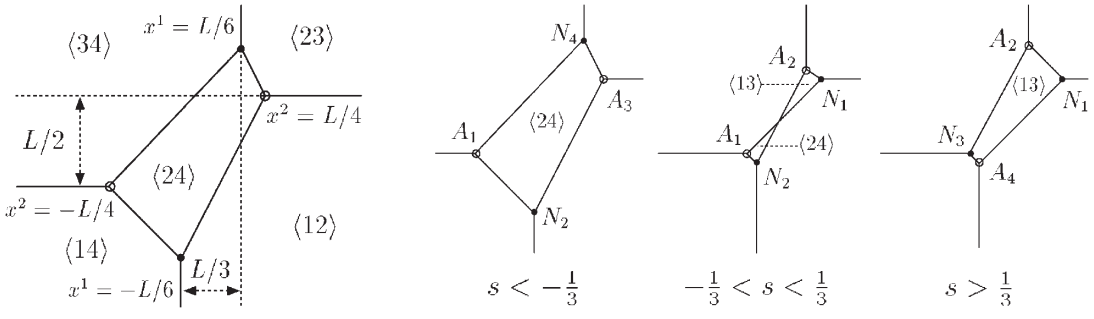

(a) A configuration (b) Deformation of the loop in the web

FIG. 12. The web diagrams in the parallelogram-type mass arrangement. Positions of the Abelian junction A_* and the non-Abelian junction N_* are given by $A_1 = (s-1, -1)$, $A_2 = (\frac{2}{3}, \frac{4}{3} + s)$, $A_3 = (\frac{1-s}{2}, 1)$, $A_4 = (-\frac{2}{3}, -\frac{2}{3} - s)$, $N_1 = (1 + s, 1)$, $N_2 = (-\frac{2}{3}, s - \frac{4}{3})$, $N_3 = (-\frac{1+s}{2}, -1)$, $N_4 = (\frac{2}{3}, \frac{2}{3} - s)$ in units of $\frac{L}{4}$.

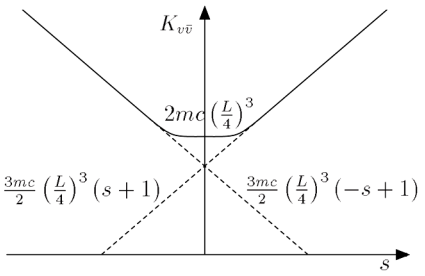

(a) The metric of the moduli space

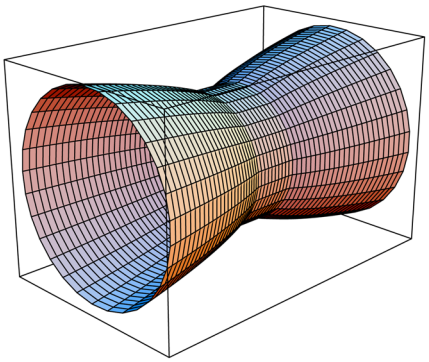

(b) The moduli space embedded into $\mathbf{R}^3$.

FIG. 13 (color online). (a) The metric evaluated numerically (solid line) and the asymptotic metric (5.8) computed from kinetic energies (dotted lines). (b) Embedding of the moduli space into the 3-dimensional Euclidean space. Here the metric is numerically evaluated in the limit $g \to \infty$. The moduli space is nonsingular since the curvature is finite everywhere.

a quadrangle loop appear as s changes, as shown in Fig. 12. The parameter θ is related to the Nambu-Goldstone mode corresponding to one of the broken flavor symmetries.

Now let us discuss the dynamics of the non-Abelian loop. If we calculate the kinetic energies of domain walls separately in the three configurations in Fig. 12, the asymptotic metric on the moduli space of the quadrangle loop is obtained as

$$\begin{aligned} ds_{\mathrm{w}}^2 &= \frac{3mc}{2}\left(\frac{L}{4}\right)^3(s+1)(ds^2+d\theta^2), \qquad s \gg \frac{1}{3}, \\ ds_{\mathrm{w}}^2 &= 2mc\left(\frac{L}{4}\right)^3(ds^2+d\theta^2), \qquad s \approx 0, \\ ds_{\mathrm{w}}^2 &= \frac{3mc}{2}\left(\frac{L}{4}\right)^3(-s+1)(ds^2+d\theta^2), \qquad s \ll -\frac{1}{3}. \end{aligned} \tag{5.8}$$

In the outer two regions of the parameter s, the metric has linear dependence on s since the lengths of the internal walls depend linearly on s. We have observed the same feature in the case of the triangle loop in Eq. (2.28). In the middle region, the linear dependence on s cancels out and the metric does not depend on s. Figure 13(a) shows the numerically evaluated metric and Fig. 13(b) shows the shape of the moduli space isometrically embedded into the 3-dimensional Euclidean space.

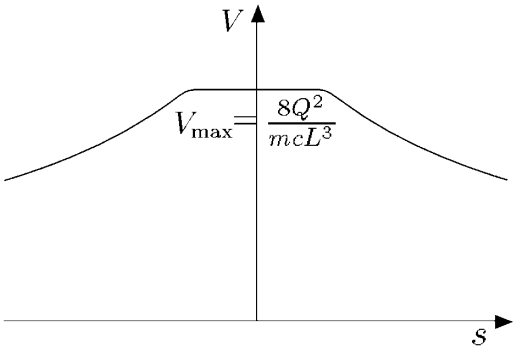

FIG. 14. The potential $V = \frac{Q^2}{4K_{v\bar{v}}}$.

If we consider the motion without flavor charge from the outer regions of the parameter s to the direction of middle region, it goes through the middle regions and continues to go in the same direction. This motion corresponds to the motion of the loop changing the vacuum region inside the loop. If the configuration has nonzero flavor charge $Q \neq 0$, the potential term $V = \frac{Q^2}{4K_{v\bar{v}}}$ will be induced in the effective Lagrangian. The typical form of the potential is shown in Fig. 14. If the energy E is greater than $V_{\max} \equiv \frac{8Q^2}{mcL^3}$, the change of the vacua inside the loop can occur as in the case of $Q = 0$. However, if $E < V_{\max}$, the quadrangle loop bounces back to be larger without changing the vacua inside the loop.

Let us next compute the kinetic energies of junctions. The magnitude of the junction charge is proportional to the area of the corresponding triangle in the grid diagram in the complex $\mathrm{Tr}\langle\Sigma\rangle$ plane. See Eqs. (2.15) and (2.17). We show the areas of four junctions in Fig. 15. The sign of the Abelian junction is minus while that of the non-Abelian junction is plus. Although the total junction charge is zero in all three regions of the parameter s, the positions of junctions have different dependence on s. This causes the different velocities of junctions for a given value of $\frac{ds}{dt}$, and the total kinetic energies of junctions can be nonzero. Since the Abelian junction transforms into the non-Abelian junction and vice versa at $s = \pm 1/3$, the kinetic energies of junctions are different in these three regions. These kinetic energies imply the additional contributions to the asymptotic metric as

$$\begin{aligned} ds_{\mathrm{j}}^2 &= -\frac{3}{8g^2}\left(\frac{L}{4}\right)^2\Delta_{[134]}(ds^2+d\theta^2), \qquad s \gg \frac{1}{3}, \\ ds_{\mathrm{j}}^2 &= 0, \qquad s \approx 0, \\ ds_{\mathrm{j}}^2 &= \frac{3}{8g^2}\left(\frac{L}{4}\right)^2\Delta_{[134]}(ds^2+d\theta^2), \qquad s \ll -\frac{1}{3}. \end{aligned} \tag{5.9}$$

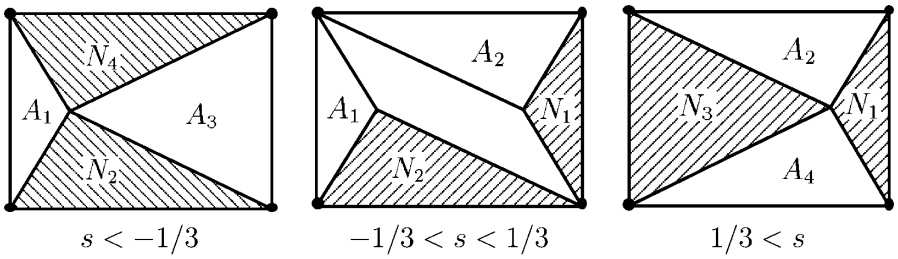

FIG. 15. The magnitude of the junction charge is proportional to the area of the triangle in the complex $\mathrm{Tr}\langle\Sigma\rangle$ plane which is dual to the junction point in the actual configuration. Abelian junctions A_i and non-Abelian junctions N_i $(i = 1, \cdots, 4)$ are illustrated in Fig. 12. Non-Abelian junctions are denoted by shaded regions.

VI. SIZE MODULUS STABILIZATION AND Q WEBS OF WALLS

So far, we have seen that the sizes of the loops tend to become larger after sufficiently long time interval. In this section, we show that the sizes of the loops stabilize if the third mass parameters M_3 are turned on in the Lagrangian (2.1). One way to introduce M_3 consistently with supersymmetry is the Scherk-Schwarz dimensional reduction from $3+1$ dimensions to $2+1$ dimensions for the Lagrangian (2.1). Then the third (twisted) mass parameter M_3 is naturally introduced together with the third adjoint scalar Σ_3 whose origin is the gauge field of the reduced dimension. Keep in mind that this explanation is merely technical in order to be compatible with supersymmetry. Once we forget about supersymmetry, the third masses can be always introduced in $3+1$ dimensions.

A. Effective theory analysis

Let us consider the triangle loop discussed in Sec. III for simplicity. If we turn on a small third mass parameter such that $M_3 = \mathrm{diag}(0, 0, 0, m_3)$, a potential $V_m(r)$ is induced in the effective theory. We can show that this potential can be obtained from the $1+1$ dimensional effective theory $\mathcal{L} = K_{w\bar{w}}(\partial_\mu r \partial^\mu r + \partial_\mu \theta \partial^\mu \theta)$ by requiring $r(t, x^3) = r(t)$, $\theta(t, x^3) = \theta(t) + m_3 x^3$ and then reducing to 1-dimensional theory as

$$L = K_{w\bar{w}}(r)\left[\left(\frac{dr}{dt}\right)^2 + \left(\frac{d\theta}{dt}\right)^2\right] - V_m(r), \qquad V_m(r) = (m_3)^2 K_{w\bar{w}}(r). \tag{6.1}$$

The asymptotic form of this potential obtained from the asymptotic Kähler metric (2.28) takes the form

$$V_m(r) = (m_3)^2 \frac{c}{2\Delta_{[123]}} \frac{r}{\alpha_1\alpha_2\alpha_3}, \tag{6.2}$$

which is valid for $r \gg 1$. This is a confining potential so that the loop shrinks and eventually shrinks to a point, if we do not turn on the flavor Q-charges coming from the motion of the phase. This potential can be interpreted as a shift of energies of the walls. Because of the small mass parameter m_3, the tensions of walls shift as[7]

$$\Delta T^{\langle A,4\rangle} = \sqrt{(T^{\langle A,4\rangle})^2 + (m_3 c)^2} - T^{\langle A,4\rangle} \approx \frac{(m_3 c)^2}{2T^{\langle A,4\rangle}}. \tag{6.3}$$

Therefore the total shift of energy can be evaluated by using Eq. (3.12) as

$$\sum_{A=1}^{3} \Delta T^{\langle A,4\rangle} l^{\langle A,4\rangle} = (m_3)^2 \frac{c}{2\Delta_{[123]}} \frac{r}{\alpha_1\alpha_2\alpha_3}. \tag{6.4}$$

When we turn on the flavor charge Q around the domain walls composing the loop given in Eq. (3.2), the effective Lagrangian can be rewritten as

$$\tilde{L} = K_{w\bar{w}}(r)\left(\frac{dr}{dt}\right)^2 - V_Q(r) - V_m(r), \tag{6.5}$$

$$V_Q(r) + V_m(r) = \frac{Q^2}{4K_{w\bar{w}}} + (m_3)^2 K_{w\bar{w}} \geq |m_3 Q|. \tag{6.6}$$

Let us remember that $K_{w\bar{w}}$ vanishes in the limit of $r \to -\infty$ and diverges in the limit of $r \to \infty$. Therefore, $V_Q(r) \equiv \frac{Q^2}{4K_{w\bar{w}}}$ increases as $r \to -\infty$ while $V_m(r) \equiv (m_3)^2 K_{w\bar{w}}$ increases as $r \to \infty$ asymptotically, and there is the minimum of the potential saturating the inequality in the last equation, as shown in Fig. 16. At the minimum, the value of the Kähler potential is related to the given Q-charge

$$K_{w\bar{w}} = \frac{1}{2}\left|\frac{Q}{m_3}\right|. \tag{6.7}$$

Comparing this with the Q-charge for the unstable con-

[7]The Scherk-Schwarz dimensional reduction just introduces one more component of the energy density for the tension T_w of domain walls in Eq. (2.8). The tension of domain walls is formally still given by the same formula, proportional to the length of the mass vector: $T^{\langle A,B\rangle} = c|\vec{m}_A - \vec{m}_B|$, except that the mass vector $\vec{m}_A$ now becomes a three-vector in the three-dimensional grid diagram, after the Scherk-Schwarz dimensional reduction.

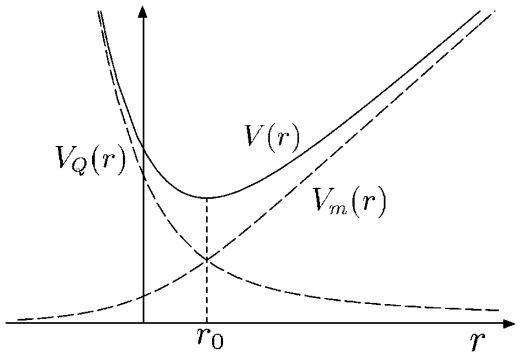

FIG. 16. The potential V for a nonzero third mass parameter m_3 and flavor charge Q. The potential V is the sum of $V_m = (m_3)^2 K_{w\bar{w}}$ and $V_Q = \frac{Q^2}{4K_{w\bar{w}}}$. The potential takes the minimum $|m_3 Q|$ at $r = r_0$.

figuration in Eq. (3.2), we observe that the stable configuration has $d\theta/dt = \pm m_3$. The relation (6.7) implies the size of the loop is stabilized at a certain value $r = r_0$. For a sufficiently small value of $|m_3|$ and large value of $|Q|$, the stabilized size r_0 takes a large value, so that it can be evaluated from the asymptotic potential as

$$r_0 = \frac{|Q|}{|m_3|c}\Delta_{[123]}\alpha_1\alpha_2\alpha_3. \tag{6.8}$$

Thus the third mass parameter M_3 stabilizes the size moduli of loops by preventing the loops from expanding forever. When the flavor charge Q becomes nonzero, the configuration is stabilized at a finite size of the loop, rather than at the boundary of the moduli space corresponding to the complete shrinkage (vanishing size) of the loop. This stabilization mechanism is the same as the one of the Q-lumps in nonlinear sigma models with a potential term [23–25]; the sizes of the Q-lumps are stabilized by the Q-charge and the masses.

In the subsequent section we will show the BPS nature of this stabilized loop configuration from the viewpoint of original theory. There we will see the origin of the minimum of the potential (6.6) which is always positive except for the case $Q = 0$ or $m_3 = 0$. The value of the potential $|Qm_3|$ at the minimum is shown to be equal to an increase in the BPS mass from the BPS loop with $Q = m_3 = 0$.

B. Q-domain wall web as 1/4 BPS soliton

So far we have seen dynamics of Q-charged domain walls and their networks mainly from the viewpoint of the low-energy effective theory. Let us go back to the original theory and reanalyze the stable network with nonzero Q-charges in more detail. It turns out that the configuration is a solution of other 1/4 BPS equations which are deformed from Eqs. (2.4) and (2.5). In order to see it, let us consider a supersymmetric model in $d = 2 + 1$ with 8 supercharges in which there is an additional adjoint scalar Σ_3 and third mass parameter M_3 as mentioned above.

It is convenient to write the mass matrix as $M_3 \equiv \mathrm{m}_3^a \mathrm{H}_a = \mathrm{diag}(m_3^1, m_3^2, \cdots, m_3^{N_\mathrm{F}})$, where we set $\mathrm{Tr} M_3 = 0$ without loss of generality and H_a $(a = 1, 2, \cdots, N_\mathrm{F} - 1)$ are the generators of $U(1)^{N_\mathrm{F}-1}$, that is, the elements of the Cartan subalgebra of $SU(N_\mathrm{F})$. The densities of conserved charges of the $U(1)^{N_\mathrm{F}-1}$ symmetries are defined by

$$\rho_a \equiv i(H^1 \mathrm{H}_a (\mathcal{D}_0 H^1)^\dagger - \mathcal{D}_0 H^1 \mathrm{H}_a H^{1\dagger}). \tag{6.9}$$

In addition, it is convenient to define an electric charge density as

$$\rho_e \equiv \partial_\alpha \mathrm{Tr}(F_{0\alpha}\Sigma_3). \tag{6.10}$$

Then the energy density can be written as

$$\begin{aligned}
\mathcal{E} &= \mathrm{Tr}\Big[\frac{1}{g^2}F_{\tilde{\alpha}0}^2 + \frac{1}{g^2}F_{12}^2 + \frac{1}{g^2}(\mathcal{D}_0\Sigma_{\tilde{\alpha}})^2 + \frac{1}{g^2}(\mathcal{D}_\alpha\Sigma_{\tilde{\alpha}})^2 - \frac{1}{2g^2}[\Sigma_{\tilde{\alpha}}, \Sigma_{\tilde{\beta}}]^2 + |\mathcal{D}_0 H^1|^2 + |\mathcal{D}_\alpha H^1|^2 \\
&\quad + |H^1 M_{\tilde{\alpha}} - \Sigma_{\tilde{\alpha}} H^1|^2 + \frac{g^2}{4}(H^1 H^{1\dagger} - c\mathbf{1}_{N_\mathrm{C}})^2\Big] \\
&= \mathrm{Tr}\Big[\frac{1}{g^2}(F_{12} - i[\Sigma_1, \Sigma_2])^2 + \frac{1}{g^2}\Big(\mathcal{D}_1\Sigma_1 + \mathcal{D}_2\Sigma_2 - \frac{g^2}{2}(c\mathbf{1}_{N_\mathrm{C}} - H^1 H^{1\dagger})\Big)^2 + \frac{1}{g^2}(\mathcal{D}_1\Sigma_2 - \mathcal{D}_2\Sigma_1)^2 \\
&\quad + |\mathcal{D}_\alpha H^1 - (H^1 M_\alpha - \Sigma_\alpha H^1)|^2 + \frac{1}{g^2}(F_{\alpha 0} + \mathcal{D}_\alpha\Sigma_3)^2 + \frac{1}{g^2}(\mathcal{D}_0\Sigma_\alpha + i[\Sigma_3, \Sigma_\alpha])^2 + \frac{1}{g^2}(\mathcal{D}_0\Sigma_3)^2 \\
&\quad + |\mathcal{D}_0 H^1 - i(H^1 M_3 - \Sigma_3 H^1)|^2\Big] + \mathcal{Y} + \mathcal{Z}_1 + \mathcal{Z}_2 + \mathrm{m}_3^a\rho_a + \frac{2}{g^2}\rho_e + \partial_\alpha J_\alpha \\
&\geq \mathcal{Y} + \mathcal{Z}_1 + \mathcal{Z}_2 + \mathrm{m}_3^a\rho_a + \frac{2}{g^2}\rho_e + \partial_\alpha J_\alpha,
\end{aligned} \tag{6.11}$$

where α stands for indices 1, 2 while $\tilde{\alpha}$ for 1, 2, 3, and we have used the Gauss's law

$$\mathcal{D}_\alpha F_{\alpha 0} - i[\Sigma_{\tilde{\alpha}}, \mathcal{D}_0\Sigma_{\tilde{\alpha}}] - i\frac{g^2}{2}(H^1\mathcal{D}_0 H^{1\dagger} - \mathcal{D}_0 H^1 H^{1\dagger}) = 0. \tag{6.12}$$

The BPS equations are obtained by requiring the BPS bound to be saturated. Apart from the equations to determine time-dependence, we find the same five 1st order equations as Eqs. (2.4) and (2.5) for the fields $\{W_\alpha, \Sigma_\alpha, H^1\}$:

$$
\begin{aligned}
&F_{12} - i[\Sigma_1, \Sigma_2] = 0, \\
&\mathcal{D}_1\Sigma_2 - \mathcal{D}_2\Sigma_1 = 0, \\
&\mathcal{D}_1\Sigma_1 + \mathcal{D}_2\Sigma_2 = \frac{g^2}{2}(c\mathbf{1}_{N_C} - H^1H^{1\dagger}), \\
&\mathcal{D}_1H^1 - H^1M_1 + \Sigma_1H^1 = 0, \\
&\mathcal{D}_2H^1 - H^1M_2 + \Sigma_2H^1 = 0.
\end{aligned}
\tag{6.13}
$$

Then the solution, except for time dependence, can be written by using the solution of the master equation Eq. (2.13) $\Omega \equiv SS^\dagger$ as Eqs. (2.9) and (2.10). Time dependence of all the fields including new variables $\{W_0, \Sigma_3\}$ are determined by additional equations [25]

$$
\begin{aligned}
&F_{\alpha 0} + \mathcal{D}_\alpha\Sigma_3 = 0, \qquad \mathcal{D}_0\Sigma_\alpha + i[\Sigma_3, \Sigma_\alpha] = 0, \\
&\mathcal{D}_0\Sigma_3 = 0, \qquad \mathcal{D}_0H^1 - iH^1M_3 + i\Sigma_3H^1 = 0.
\end{aligned}
\tag{6.14}
$$

If we choose a gauge such that $W_0 = -\Sigma_3$, these can be solved by replacing H_0 as $H_0 \to H_0e^{iM_3t}$ and requiring the other fields to be independent of time:

$$
\begin{aligned}
&iW_1 + \Sigma_1 = S^{-1}\partial_1 S, \qquad iW_2 + \Sigma_2 = S^{-1}\partial_2 S, \\
&H^1 = S^{-1}H_0e^{M_1x^1 + M_2x^2 + iM_3t}.
\end{aligned}
\tag{6.15}
$$

The spatial profile of the gauge field W_0 (and adjoint scalar Σ_3) are finally determined from the Gauss's law constraint Eq. (6.12). The solution takes the form of

$$
W_0 = -\Sigma_3 = -\mathrm{m}_3^a\left(\frac{\partial}{\partial\sigma^a}S^\dagger S^{\dagger -1} + S^{-1}\frac{\partial}{\partial\bar{\sigma}^a}S\right). \tag{6.16}
$$

Here, σ^a $(a = 1, 2, \cdots, N_F - 1)$ are the complex moduli parameters whose imaginary parts correspond to the Nambu-Goldstone modes of $U(1)^{N_F-1}$ symmetries, that is, σ^a appear in the expression of H_0 as $H_0(\sigma^a) = H_0(\sigma^a = 0)e^{\sigma^a\mathrm{H}_a}$. It is instructive to note a similarity between Eqs. (2.24) and (6.16). Recall that the latter is the solution of the Gauss's law constraint for the configurations when we promote the moduli parameters of the stationary 1/4 BPS background to fields (functions of the world volume coordinates including time $t = x^{\mu=0}$). Let us suppose that we make an ansatz for the field σ^a to depend only linearly on time as $\sigma^a(t) = \sigma^a + i\mathrm{m}_3^at$, namely, the moduli matrix changes as $H_0e^{\sigma^a\mathrm{H}_a} \to H_0e^{\mathrm{H}_a(\sigma^a + i\mathrm{m}_3^at)}$. This leads to $\partial_0\sigma^a(t) = i\mathrm{m}_3^a$ and then the solution (2.24) corresponds to the solution (6.16).

For the solution Eqs. (6.15) and (6.16), the Q-charges are determined by integrating the densities $Q_a = \int d^2x\rho_a$. Interestingly, the Q-charge which is a variable defined in the original theory can be directly related to the Kähler metric of the low-energy effective theory (2.25)

$$
\begin{aligned}
&Q_a = 2\mathrm{m}_3^bK_{a\bar{b}} = 2\mathrm{m}_3^bK_{b\bar{a}}, \\
&K_{a\bar{b}} \equiv \frac{\partial}{\partial\bar{\sigma}^b}\frac{\partial}{\partial\sigma^a}K = K_{b\bar{a}}.
\end{aligned}
\tag{6.17}
$$

Here we have used the fact that the Kähler potential K is independent of the imaginary parts of σ^a. Since the right-hand side depends on the parameters contained in H_0, some of these parameters are fixed for given values of Q_a. Therefore, those parameters are no longer moduli parameters and the configuration is stabilized. Especially, in the case of the triangle loop discussed in the previous subsection, we can show that the size parameter is fixed at the same value obtained as the minimum of the potential Eq. (6.7) in the effective theory by taking, for example, $\sigma^a = (0, 0, \sqrt{\frac{3}{2}}w)$ and $\mathrm{m}_3^a = (0, 0, \sqrt{\frac{3}{2}}m_3)$ with $\mathrm{H}_{a=3} = \frac{1}{2\sqrt{6}}\mathrm{diag}(-1, -1, -1, 3)$ and the notation $Q = \sqrt{\frac{3}{2}}Q_{a=3}$. Furthermore, the minimum value $|m_3Q|$ of the effective potential in Eq. (6.6) precisely corresponds to the increment of energy bound $\mathrm{m}_3^aQ_a$ in the last line of Eq. (6.11). Note that since $F_{0\alpha} \to 0$ at spatial infinity in this case, the electric charge does not contribute to the total energy.[8] Eq. (6.17) tells us that the 1/4 BPS configuration requires both nonzero Q-charges and the third masses m_3^a (or both of them to vanish simultaneously). If one of them is absent, the balance between them is lost and the configuration no longer is BPS. This is also consistent with what we found from the effective theory viewpoint in the previous sections.

VII. CONCLUSION AND DISCUSSION

In this paper, we investigated dynamics of 1/4 BPS domain wall networks (or webs) in Abelian or non-Abelian gauge theories coupled with complex masses for Higgs fields in the fundamental representation. In the previous paper [6] we have obtained the effective action on the world volume of the domain wall networks. In this paper we applied it to study the dynamics of the networks. Namely, we described the dynamics of the slowly moving networks as geodesics on their moduli space, namely, with the moduli approximation. Only moduli parameters related to internal loops composed of several domain walls in the networks can be treated as massless fields in the effective Lagrangian. Other moduli are associated with the shift of external domain walls, which requires an infinite amount of energy and results in the change of boundary conditions.

As concrete examples, we dealt with three different types of loops in Abelian or non-Abelian gauge theories. The first example is in Sec. III where the simplest configuration of the single triangle loop appears in the Abelian gauge theory with 4 massive Higgs fields. The metric of the moduli space for the single loop has a geometry between a cone and a cigar [6]. We found geodesics corresponding to any motion of a shrinking loop pass the tip (zero size of the loop). This means that the loop bounces back with π rotation of the internal phase and eventually expands to

[8]The Q-wall can be viewed as a capacitor with electric charge distributions on the two sides of the wall [31]. Since these charges have opposite signs, the total electric charge vanishes.

an infinite loop. The second example is the dynamics of two loops in the Abelian gauge theory with 6 massive Higgs fields in Sec. IV. There exist seven types of configurations shown in Fig. 9. We numerically showed that after a sufficiently long time both of the two loops expand forever irrespective of the initial condition. As the two loops get larger, the system approaches a system of two independent single loops. Our last example is the network including both Abelian and non-Abelian junctions which appears in the $U(2)$ gauge theory with 4 massive Higgs fields [18]; see Sec. V. After fixing all the non-normalizable moduli, there remains only one complex moduli parameter s as the normalizable modulus which controls the areas of two vacuum regions. We found the metric of the moduli space whose geometry in Fig. 13 looks like a sandglass made by gluing the tips of the two metrics of a single triangle loop in Fig. 5. The geodesic of s is a one way traffic from any initial value to an expanding loop with either $s = +\infty$ or $s = -\infty$ (one or the other branches of the sandglass), depending on its initial velocity. Namely, only one of the loop out of two loops remains after sufficient time.

We also considered the dynamics of the web loop accompanied by a phase rotation in the internal direction, a $U(1)$ isometry which originates from a linear combination of broken $U(1)$ flavor symmetries. Conserved charges associated with the rotation are Q-charges of the domain walls composing the loops. These Q-charges give a runaway potential in the effective theory and exert a repulsive force between walls in the loop. Then the loops with Q-charges are generally unstable (non-BPS) and tend to expand forever. Thanks to the repulsive force, the geodesics bounce back before reaching the completely shrunk loops. The minimum sizes of the loops are determined by the given Q-charges. For the loops including both the Abelian and the non-Abelian junctions with the sandglass geometry in Fig. 13, the corresponding geodesic motion becomes bounce back type or one way traffic type depending on the total energy and the given Q-charge.

By introducing the third masses for the Higgs fields, the effective theory of the loops acquires an attractive potential in contrast to the Q-charges. In the presence of the third masses, the loops tend to shrink. Coexistence of the Q-charges and the third masses stabilize the size of the loops. Then the size of the loop is fixed at some value where the attractive and the repulsive forces are balanced like the known stabilization mechanism of size moduli for the lumps due to the suitable potential accompanied by the Q-charge [23–25]. We also studied such configurations in the original theory, rather than in the effective theory on the world volume of the web of loops. Then we derived new $1/4$ BPS equations which includes time derivatives and found a new BPS bound which is the sum of the topological charges of domain walls and their junctions and the additional masses coming from the Q-charges. General solutions of the $1/4$ BPS equations with the Gauss's law are found. All the results found in the original theory are compatible with those found in the effective theory.

To illustrate the behavior of domain wall networks in this paper, we took the strong gauge coupling limit where the background solutions are explicitly available. This limit is sufficient to discuss qualitatively the dynamics of the networks even at finite gauge couplings. This is because the asymptotic metrics on the moduli space (large loops) are not sensitive on the gauge coupling [6]. Furthermore, when we turn on the nonzero flavor charges, the loops cannot get close to shrinking points. The flavor charges are generally produced whenever we promote the relative phase moduli to fields on the effective theories. So our analysis is adequate to know qualitative features for any gauge coupling. It is an interesting future problem to study numerically at finite gauge couplings in order to clarify more detailed aspects of the network dynamics.

Here we make several comments on possible extensions of the present work.

Global cosmic strings appear when global $U(1)$ symmetry is spontaneously broken. It is well-known that there exists a repulsive force between two strings. Strings interact with the Nambu-Goldstone boson associated with the spontaneously broken $U(1)$ symmetry, and the repulsive force was explained in terms of the Nambu-Goldstone bosons propagating in the bulk [2]. In the same way, it will be possible to explain the repulsive force induced inside a domain wall loop in terms of the Nambu-Goldstone bosons. A feature different from the case of cosmic strings is that the Nambu-Goldstone modes in this case of a domain wall loop are normalizable and therefore appear in the low-energy effective action of the loop as shown in this paper.

An extension to a supertube [32] is interesting and may have some impact on string theory. With a Noether charge density, domain walls with arbitrary shape [33] were constructed as a field theory realization of a supertube. Our work should be extendible to a BPS supertube junction. Such a solution may suggest a junction of a membrane tube in M-theory. In fact, the junction of membranes was already constructed in $d = 6$, $\mathcal{N} = (2, 0)$ supersymmetric theories [34].

It is interesting to explore applications of our results to cosmology. Our theory is supersymmetric and all stationary configurations discussed in this paper are BPS and are stable. In the early Universe supersymmetry is expected to be unbroken. Therefore our results can be applied when gauge and global symmetry are broken above the supersymmetry breaking scale. Vacuum regions inside domain wall loops are considered to be bubbles. Our results imply all bubbles grow for a late time in theory with complex masses if the size of the Universe is infinite. In this respect, it is worth generalizing our work to domain wall webs in a finite size space. In this case, zero modes of external legs of walls become normalizable and are promoted to fields in

the effective theory. Dynamics of webs is not restricted to loops and will become richer. If we do not restrict ourselves to a supersymmetric Universe, we can allow triplet masses of Higgs fields even in four space-time dimensions. In this case, the bubble (loop) sizes are stabilized. Growing bubbles with (without) a Q-charge will be stabilized (shrink) after supersymmetry is broken and the triplet masses are induced.

ACKNOWLEDGMENTS

This work is supported in part by Grants-in-Aid for Scientific Research from the Ministry of Education, Culture, Sports, Science, and Technology, Japan, Nos. 17540237 and 18204024 (N. S.). The work of T. F. is supported by the Japan Society for the Promotion of Science for Young Scientists. The work of M. E. and K. O. is also supported by the Japan Society for the Promotion of Science for Research Abroad. T. N. gratefully acknowledges support from a 21st Century COE Program at Tokyo Tech, "Nanometer-Scale Quantum Physics," by the Ministry of Education, Culture, Sports, Science, and Technology, and support from the Iwanami Fujukai Foundation.

APPENDIX: TRIANGLE LOOP WITH DEGENERATE MASSES

Let us consider a triangle loop for $N_C = 1$, $N_F = 5$ case in which the masses for fourth and fifth flavor components are degenerate, $\vec{m}_4 = \vec{m}_5$. There exist four Killing vector fields ξ_0, ξ_a $(a = 1, 2, 3)$ on the moduli space, which are given by

$$\xi_0 \equiv i\phi^i\partial_i + (\text{c.c.}), \qquad \xi_a \equiv i(\sigma_a)_{ij}\phi^j\partial_i + (\text{c.c.}). \tag{A1}$$

These Killing vectors originate from the $U(2)$ flavor symmetry which rotates the fourth and fifth flavor components of H. Not all of them are independent. Instead they are related as

$$\xi_0 = \frac{1}{|\boldsymbol{\phi}|^2}(\bar{\phi}\sigma_a\phi)\xi_a. \tag{A2}$$

The tangent space of the moduli space can be orthogonally decomposed into the direction of size of the loop $t_r \equiv \phi^i\partial_i + (\text{c.c.})$, phase of the loop $t_\theta \equiv \xi_0$, and two directions of the vacuum moduli inside the loop $t_I \equiv c_I^a\xi_a$ $(I = 1, 2)$. Here the coefficients c_I^a are defined by $c_I^a(\bar{\phi}\sigma^a\phi) = 0$, $c_I^a c_J^a = \delta_{IJ}$. The norms of these vector fields are given by

$$\begin{aligned}\|t_r\|^2 = \|t_\theta\|^2 &= 2|\boldsymbol{\phi}|^2(K'(|\boldsymbol{\phi}|^2) + |\boldsymbol{\phi}|^2K''(|\boldsymbol{\phi}|^2)) \\ &= \frac{1}{2}\frac{\partial^2}{\partial r^2}K,\end{aligned} \tag{A3}$$

$$\|t_1\|^2 = \|t_2\|^2 = 2|\boldsymbol{\phi}|^2K'(|\boldsymbol{\phi}|^2) = \frac{\partial}{\partial r}K, \tag{A4}$$

Here $r \equiv \log|\boldsymbol{\phi}|$ can be interpreted as the size of the loop. For large r, $K \to \frac{c}{3\Delta_{[123]}}\frac{1}{\alpha_1\alpha_2\alpha_3}r^3$ and the norms Eqs. (A3) and (A4) become

$$\begin{aligned}\|t_r\|^2 = \|t_\theta\|^2 &\to \frac{c}{\Delta_{[123]}}\frac{r}{\alpha_1\alpha_2\alpha_3}, \\ \|t_1\|^2 = \|t_2\|^2 &\to \frac{c}{\Delta_{[123]}}\frac{r^2}{\alpha_1\alpha_2\alpha_3}.\end{aligned} \tag{A5}$$

These asymptotic forms of the norms and their dependence on the size of the loop r show the fact that the metric densities for size and phase moduli have a one-dimensional support on the edges of the loop, while those for the vacuum moduli have a two-dimensional support extended fully inside the loop (see Fig. 4). Since the moduli space has isometrics generated by the Killing vectors ξ_0 and ξ_a, there are conserved Noether charges defined by

$$Q = \langle\dot{\phi}, \xi_0\rangle = iK_{i\bar{j}}(\dot{\bar{\phi}}^j\phi^i - \dot{\phi}^i\bar{\phi}^j), \tag{A6}$$

$$q_a = \langle\dot{\phi}, \xi_a\rangle = iK_{i\bar{j}}(\dot{\bar{\phi}}^j(\sigma_a)^i{}_k\phi^k - \dot{\phi}^i\bar{\phi}^k(\sigma_a)_k{}^j), \tag{A7}$$

where $\dot{\phi} \equiv \dot{\phi}^i\partial_i + (\text{c.c.})$ and $\langle\,,\,\rangle$ denotes the inner product with respect to the metric of the moduli space $K_{i\bar{j}}$. These conserved charges are related as

$$Q = \frac{1}{|\boldsymbol{\phi}|^2}(\bar{\phi}\sigma_a\phi)q_a. \tag{A8}$$

Since the tangent vectors t_r, t_θ, t_1, t_2 are orthogonal, the time derivative of the moduli parameters $\dot{\phi}$ can be written as

$$\dot{\phi} = \frac{\langle\dot{\phi}, t_r\rangle}{\|t_r\|^2}t_r + \frac{\langle\dot{\phi}, t_\theta\rangle}{\|t_r\|^2}t_\theta + \frac{\langle\dot{\phi}, t_1\rangle}{\|t_1\|^2}t_1 + \frac{\langle\dot{\phi}, t_2\rangle}{\|t_2\|^2}t_2. \tag{A9}$$

Then the energy in the effective theory can be written as

$$\begin{aligned}E &= \frac{1}{2}\langle\dot{\phi}, \dot{\phi}\rangle \\ &= \frac{1}{2}\left(\frac{\langle\dot{\phi}, t_r\rangle^2}{\|t_r\|^2} + \frac{\langle\dot{\phi}, t_\theta\rangle^2}{\|t_\theta\|^2} + \frac{\langle\dot{\phi}, t_1\rangle^2}{\|t_1\|^2} + \frac{\langle\dot{\phi}, t_2\rangle^2}{\|t_2\|^2}\right) \\ &= \frac{1}{4}\partial_r^2K\dot{r}^2 + \frac{Q^2}{\partial_r^2K} + \frac{1}{2\partial_rK}(c_1^ac_1^b + c_2^ac_2^b)q_aq_b \\ &= \frac{1}{4}\partial_r^2K\dot{r}^2 + \left(\frac{1}{\partial_r^2K} - \frac{1}{2\partial_rK}\right)Q^2 + \frac{q_aq_a}{2\partial_rK}.\end{aligned} \tag{A10}$$

Here we have used $\langle\dot{\phi}, t_r\rangle = \dot{r}\|t_r\|^2$ and $c_1^ac_1^b + c_2^ac_2^b + (\bar{\phi}\sigma^a\phi)(\bar{\phi}\sigma^b\phi)/|\boldsymbol{\phi}|^4 = \delta^{ab}$.

[1] T. W. B. Kibble, J. Phys. A **9**, 1387 (1976).

[2] A. Vilenkin and E. P. S. Shellard, *Cosmic Strings and Other Topological Defects* (Cambridge University Press, Cambridge, UK, 1994).

[3] M. Bucher and D. N. Spergel, Phys. Rev. D **60**, 043505 (1999); R. A. Battye, M. Bucher, and D. Spergel, arXiv:astro-ph/9908047; A. Friedland, H. Murayama, and M. Perelstein, Phys. Rev. D **67**, 043519 (2003); L. Campanelli, P. Cea, G. L. Fogli, and L. Tedesco, Int. J. Mod. Phys. D **14**, 521 (2005); L. Conversi, A. Melchiorri, L. Mersini-Houghton, and J. Silk, Astropart. Phys. **21**, 443 (2004); J. C. R. Oliveira, C. J. A. Martins, and P. P. Avelino, Phys. Rev. D **71**, 083509 (2005); P. P. Avelino, J. C. R. Oliveira, and C. J. A. Martins, Phys. Lett. B **610**, 1 (2005); P. P. Avelino, C. J. A. Martins, and J. C. R. Oliveira, Phys. Rev. D **72**, 083506 (2005); P. Pina Avelino, C. J. A. Martins, J. Menezes, R. Menezes, and J. C. R. Oliveira, Phys. Rev. D **73**, 123519 (2006); **73**, 123520 (2006); B. Carter, arXiv:hep-ph/0605029; R. A. Battye, E. Chachoua, and A. Moss, Phys. Rev. D **73**, 123528 (2006); R. A. Battye and A. Moss, Phys. Rev. D **74**, 041301 (2006); **74**, 023528 (2006).

[4] N. S. Manton, Phys. Lett. **110B**, 54 (1982).

[5] N. S. Manton and P. Sutcliffe, *Topological Solitons* (Cambridge University Press, Cambridge, UK, 2004).

[6] M. Eto, T. Fujimori, T. Nagashima, M. Nitta, K. Ohashi, and N. Sakai, Phys. Rev. D **75**, 045010 (2007).

[7] Y. Isozumi, M. Nitta, K. Ohashi, and N. Sakai, Phys. Rev. Lett. **93**, 161601 (2004); Phys. Rev. D **70**, 125014 (2004); M. Eto, Y. Isozumi, M. Nitta, K. Ohashi, K. Ohta, and N. Sakai, Phys. Rev. D **71**, 125006 (2005); M. Eto, Y. Isozumi, M. Nitta, K. Ohashi, K. Ohta, N. Sakai, and Y. Tachikawa, Phys. Rev. D **71**, 105009 (2005).

[8] D. Tong, arXiv:hep-th/0509216.

[9] M. Eto, Y. Isozumi, M. Nitta, K. Ohashi, and N. Sakai, J. Phys. A **39**, R315 (2006).

[10] M. Shifman and A. Yung, arXiv:hep-th/0703267.

[11] M. Arai, M. Nitta, and N. Sakai, Prog. Theor. Phys. **113**, 657 (2005); Yad. Fiz. **68**, 1698 (2005) [Phys. At. Nucl. **68**, 1634 (2005)].

[12] Y. Isozumi, M. Nitta, K. Ohashi, and N. Sakai, in *Proceedings of 12th International Conference on Supersymmetry and Unification of Fundamental Interactions (SUSY 04), Tsukuba, Japan, 2004*, edited by K. Hagiwara *et al.* (KEK, Tsukuba, 2004) p. 1; Proceedings of ''NathFest,'' PASCOS Conference, Boston, 2004 (to be published); M. Eto, Y. Isozumi, M. Nitta, K. Ohashi, and N. Sakai, AIP Conf. Proc. **805**, 266 (2005); in *Proceedings of the Conference Continuous Advances in QCD 2006, University of Minnesota, 2006* (World Scientific, Singapore, 2007), p. 58.

[13] E. R. C. Abraham and P. K. Townsend, Phys. Lett. B **291**, 85 (1992); **295**, 225 (1992); J. P. Gauntlett, D. Tong, and P. K. Townsend, Phys. Rev. D **64**, 025010 (2001); D. Tong, Phys. Rev. D **66**, 025013 (2002); J. High Energy Phys. 04 (2003) 031; K. S. M. Lee, Phys. Rev. D **67**, 045009 (2003); M. Arai, M. Naganuma, M. Nitta, and N. Sakai, Nucl. Phys. **B652**, 35 (2003); in *Garden of Quanta—In honor of Hiroshi Ezawa*, edited by J. Arafune *et al.* (World Scientific, Singapore, 2003), p. 299; M. Arai, E. Ivanov, and J. Niederle, Nucl. Phys. **B680**, 23 (2004); Y. Isozumi, K. Ohashi, and N. Sakai, J. High Energy Phys. 11 (2003) 061; 11 (2003) 060; N. Sakai and Y. Yang, Commun. Math. Phys. **267**, 783 (2006); A. Hanany and D. Tong, Commun. Math. Phys. **266**, 647 (2006).

[14] M. Eto, Y. Isozumi, M. Nitta, K. Ohashi, and N. Sakai, Phys. Rev. Lett. **96**, 161601 (2006); M. Eto, T. Fujimori, Y. Isozumi, M. Nitta, K. Ohashi, K. Ohta, and N. Sakai, Phys. Rev. D **73**, 085008 (2006); M. Eto, K. Konishi, G. Marmorini, M. Nitta, K. Ohashi, W. Vinci, and N. Yokoi, Phys. Rev. D **74**, 065021 (2006); M. Eto, K. Hashimoto, G. Marmorini, M. Nitta, K. Ohashi, and W. Vinci, Phys. Rev. Lett. **98**, 091602 (2007); M. Eto, L. Ferretti, K. Konishi, G. Marmorini, M. Nitta, K. Ohashi, W. Vinci, and N. Yokoi, Nucl. Phys. **B780**, 161 (2007); M. Eto, J. Evslin, K. Konishi, G. Marmorini, M. Nitta, K. Ohashi, W. Vinci, and N. Yokoi, Phys. Rev. D **76**, 105002 (2007); M. Eto, T. Fujimori, M. Nitta, K. Ohashi, K. Ohta, and N. Sakai, Nucl. Phys. **B788**, 120 (2008).

[15] Y. Isozumi, M. Nitta, K. Ohashi, and N. Sakai, Phys. Rev. D **71**, 065018 (2005).

[16] M. Eto, Y. Isozumi, M. Nitta, K. Ohashi, and N. Sakai, Phys. Rev. D **72**, 025011 (2005).

[17] M. Eto, Y. Isozumi, M. Nitta, K. Ohashi, and N. Sakai, Phys. Rev. D **72**, 085004 (2005).

[18] M. Eto, Y. Isozumi, M. Nitta, K. Ohashi, and N. Sakai, Phys. Lett. B **632**, 384 (2006).

[19] M. Eto, Y. Isozumi, M. Nitta, K. Ohashi, K. Ohta, and N. Sakai, AIP Conf. Proc. **805**, 354 (2005).

[20] G. W. Gibbons and P. K. Townsend, Phys. Rev. Lett. **83**, 1727 (1999); S. M. Carroll, S. Hellerman, and M. Trodden, Phys. Rev. D **61**, 065001 (2000); A. Gorsky and M. A. Shifman, Phys. Rev. D **61**, 085001 (2000).

[21] H. Oda, K. Ito, M. Naganuma, and N. Sakai, Phys. Lett. B **471**, 140 (1999); K. Ito, M. Naganuma, H. Oda, and N. Sakai, Nucl. Phys. **B586**, 231 (2000); Nucl. Phys. B, Proc. Suppl. **101**, 304 (2001); M. Naganuma, M. Nitta, and N. Sakai, Phys. Rev. D **65**, 045016 (2002); in *Proceedings of 3rd International Sakharov Conference on Physics*, edited by A. Semikhatov *et al.* (World Scientific Pub., Singapore, 2003), p. 537.

[22] M. Eto, Y. Isozumi, M. Nitta, K. Ohashi, and N. Sakai, Phys. Rev. D **73**, 125008 (2006); N. Sakai, M. Eto, Y. Isozumi, M. Nitta, and K. Ohashi, Proc. Sci. stringsLHC (2007) 025.

[23] R. A. Leese, Nucl. Phys. **B366**, 283 (1991); E. Abraham, Phys. Lett. B **278**, 291 (1992); M. Naganuma, M. Nitta, and N. Sakai, Gravitation Cosmol. **8**, 129 (2002); D. Bak, S. O. Hahn, J. Lee, and P. Oh, Phys. Rev. D **75**, 025004 (2007).

[24] K. M. Lee and H. U. Yee, Phys. Rev. D **72**, 065023 (2005).

[25] M. Eto, Y. Isozumi, M. Nitta, and K. Ohashi, Nucl. Phys. **B752**, 140 (2006).

[26] D. Tong, Phys. Lett. B **460**, 295 (1999); D. Bak, C. k. Lee, K. M. Lee, and P. Yi, Phys. Rev. D **61**, 025001 (1999).

[27] N. D. Lambert and D. Tong, Phys. Lett. B **462**, 89 (1999); K. Peeters and M. Zamaklar, J. High Energy Phys. 12 (2001) 032.

[28] U. Lindström and M. Roček, Nucl. Phys. **B222**, 285 (1983); I. Antoniadis and B. Pioline, Int. J. Mod. Phys. A **12**, 4907 (1997).

[29] M. Shifman and A. Yung, Phys. Rev. D **70**, 025013 (2004).

[30] M. Eto, M. Nitta, K. Ohashi, and D. Tong, Phys. Rev. Lett. **95**, 252003 (2005).
[31] S. Bolognesi and M. Shifman, arXiv:0705.0379.
[32] D. Mateos and P. K. Townsend, Phys. Rev. Lett. **87**, 011602 (2001).
[33] S. Kim, K. M. Lee, and H. U. Yee, Phys. Rev. D **75**, 125011 (2007).
[34] K. M. Lee and H. U. Yee, J. High Energy Phys. 03 (2007) 057.